Drivers of Stable Water Isotope Anomalies in a Temperate Alaskan Ice Core on the Juneau Icefield

By
Paloma Siegel
Department of Geography, University of Colorado Boulder

April 10, 2023

Defense Committee:
Thesis Advisor: Dr. Holly Barnard, Department of Geography
Dr. Joe Bryan, Department of Geography
Dr. Bradley Markle, Department of Geological Sciences

Abstract

Ratios of stable oxygen and hydrogen isotopes in water are a well-established proxy for regional temperature and can be measured in snow and ice to reconstruct current and past climate trends. This study focuses the on Matthes-Llewelyn Ice Core, a 294m deep ice core drilled in 2019 on the Juneau Icefield. Specifically, we examine the potential drivers of measured water isotope anomalies in the upper 24.5m of the ice that coincide with the presence of liquid water in a ~5cm thick firn aquifer. We pursue two hypotheses to examine the driver(s) of these anomalies. First, we consider the influence of shifts in evaporation source temperature through storm trajectory pathway modeling and sea surface temperature (SST) analysis. Next, we consider the impact of post-depositional processes on the glacial water isotope composition because they may alter measured signals and influence how ice core water isotope records are interpreted in melt-impacted glaciers. Analysis uses the Simple Water Isotope Model (SWIM), the Hybrid Single-Particle Lagrangian Integrated Trajectory (HySPLIT) model, and National Center for Environmental Prediction (NCEP) reanalysis SST data. SWIM temperature reconstructions for the ML Ice Core water isotope record indicate that the evaporation source temperature in the upper 24.5m of the ice core decreased by approximately 5˚C. We investigate the SWIM outputs with HySPLIT modeled daily air parcel back-trajectories for one year prior to and directly after the estimated age of the ice at the firn-ice transition. We then compared the HySPLIT outputs to SST reanalysis plots to determine if storm paths shifted to a cooler location, or if specific regions of the North Pacific cooled surficially. Last, we analyzed snow and ice samples from the 2021 JIRP field season to examine potential post-depositional processes pertaining to meltwater and melt/re-freeze cycles. Combined HySPLIT modeling and SST analysis do not support the hypothesis that evaporative source temperature shifts caused the water isotope anomalies at and above the firn-ice transition, thus suggesting that post-depositional processes occurring englacially possibly led to the observed data spikes. Preliminary 2021 snow and ice lens analysis indicates that mean deuterium excess values are significantly higher in refrozen melt layers, perhaps alluding to post-depositional alteration. We cannot confirm that post-depositional processes are occurring, but we are confident that atmospheric/climatological shifts are not driving the observed anomalies.

Introduction

Ice cores are cylinders of ice collected from glaciers and icesheets worldwide and used to examine a myriad of climate dynamics. In the Pacific Northwest, they have been drilled on alpine glaciers in seven distinct locations, extending as far south as Mt. Waddington in British Columbia and as far north as the McCall Glacier in Arctic Alaska (see Fig. 1). Alpine glaciers are sensitive to multiple climatological factors including shifting lapse rates, atmospheric water vapor circulation, cloud cover, and albedo feedback systems, making these regions highly vulnerable to climate change (Winski et al., 2018).

Glacial mass loss is due in part to ice thinning and terminus retreat associated with climate warming over the past few decades (Arendt et al., 2002; Zemp et al., 2019). Arendt et al. (2002) estimated that Alaskan glacial volume loss from the mid 1950's to 2001 accounts for approximately 9% of the observed global sea-level rise through that same period. They noted that the glaciers within the Chugach Range, St. Elias Mountains, and Coast Range played the most important role. A follow-up study found that between 1961 and 2016, Alaskan glaciers made up one third of the mass loss and sea level-rise from non-polar ice sheets (Greenland and Antarctica), with "record mass losses" (Zemp et al., 2019). The meltwater input to the ocean from these Alaskan glaciers will be a significant contributor to sea level rise in the near future (Zemp et al., 2019). Melt-impacted glaciers, such as those in Southeast Alaska, store records of regional climate in their geochemical stratigraphy, which may be altered or destroyed as melt progresses. Therefore, the way we interpret ice core signals from alpine glaciers has implications for climate research and our ability to predict future conditions based on past patterns.

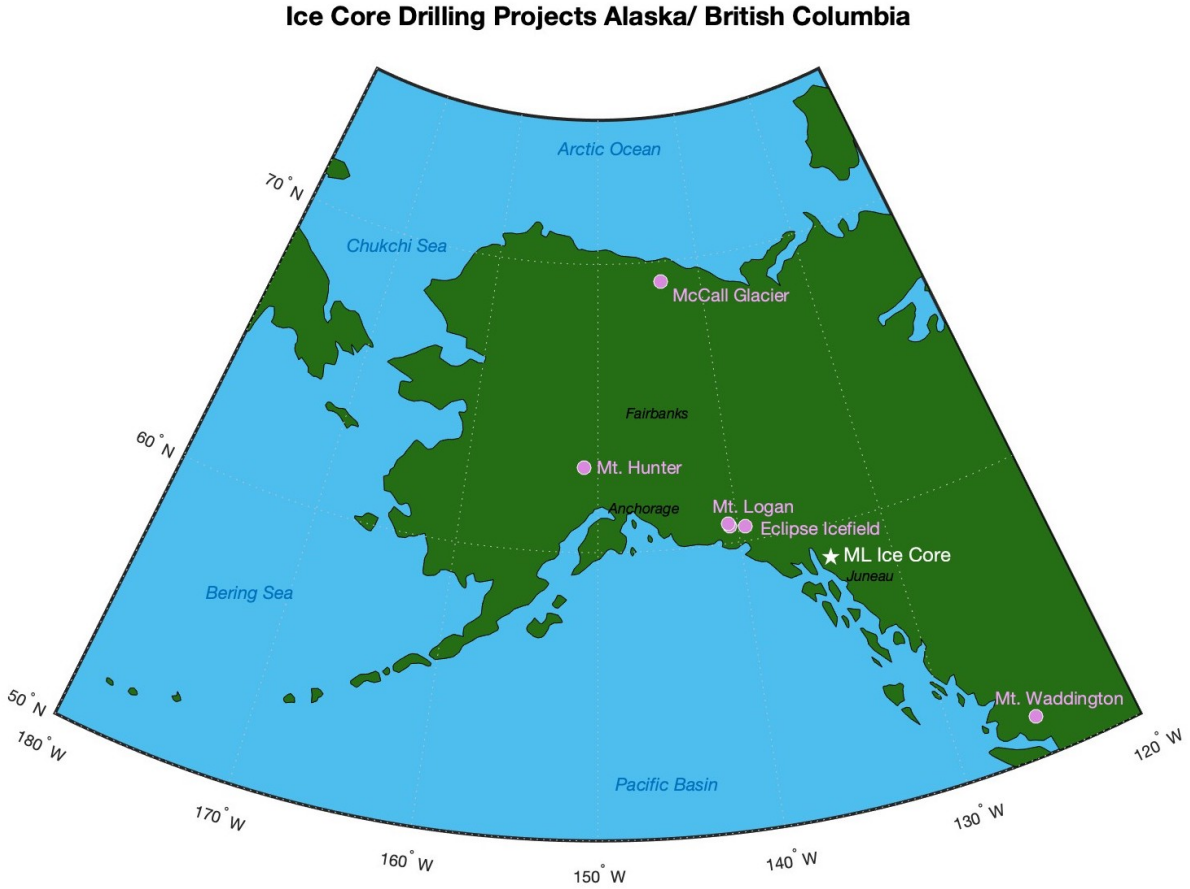

Figure 1: Map of Alaska and western British Columbia ice core sites (purple circles) and 2019 ML Ice Core site (white star).

Background

This paper explores the stable water isotope geochemistry of the 2019 Matthes-Llewelyn (ML) Ice Core and 2021 snow data collected on the Juneau Icefield in order to better understand the effects of melt and post-depositional changes to water isotope records in this region with the intention of improving climatological studies in Southeast Alaska. An improved understanding of post-depositional processes that affect water isotopes in temperate glacial ice cores will allow for more nuanced interpretations of these isotope records (Moran & Moran, 2009; Pu et al., 2020; Wahl et al, 2021).

The Juneau Icefield is situated on the southeastern coast of Alaska within the Coast Mountains, 1800m above the Pacific Ocean and tucked between jagged granite peaks. The Matthes-Llewelyn glacier divide lies near the highest ice elevation on the Juneau Icefield, from which the Llewelyn Glacier flows north into Canada and the Matthes Glacier flows south towards coastal Alaska and into the Taku Glacier. One of the thickest temperate alpine glaciers in the Northern Hemisphere, the Taku Glacier is the main artery of the Juneau Icefield. Temperate glaciers contain ice that lingers at its pressure-melting point, 0˚C, throughout its depth and are not frozen to the bedrock as is typical for polar glaciers (Anderson & Anderson, 2010; Martini et al., 2001). This characteristic, observed across the Juneau Icefield, can support higher flow velocity rates due to the presence of meltwater at the ice-rock interface (Anderson & Anderson, 2010). This research was conducted through the Juneau Icefield Research Program (JIRP), the longest continuously running glacial observation project in North America (Nolan et al., 1995; Pelto et al., 2008; *Juneau Icefield Research Program*, n.d).

Stable Water Isotope in the Hydrosphere

Stable water isotope ratios are used across many disciplines of Earth Science. In the field of paleoclimatology to examine climate dynamics such as past temperature, precipitation, and atmospheric circulation trends (Dansgaard, 1964; Jouzel & Merlivat, 1984). Elements are defined by the number of protons in the nucleus of an atom. Isotopes are atoms of the same element with different numbers of neutrons in their nuclei (Martini et al., 2001; Sharp, 2017). Adding neutrons to an atom increases its mass, and these “heavy” isotopes are rarer than “light” isotopes on Earth (see Table 1). Average abundance is determined by the average atomic mass of the isotope relative to the other isotopes of an atom (Sharp, 2017). A stable isotope is one that does not decay over time or change in atomic structure. From a mass balance perspective, stable isotopes persist in the environment and are unchanging in their absolute abundance. Any changes to a stable isotope’s relative abundance in a system is thus driven by measurable chemical, physical, and biological processes that impart fractionation (Sharp, 2017; White, 2015).

Fractionation describes the physical sorting or separation of heavy and light isotopes and is used to understand dynamics in an isotope’s relative abundance in a given system (Sharp, 2017; White, 2015).

Stable water isotope fractionation is mass dependent and controlled by factors such as temperature, altitude, continentality, latitude, and relative humidity. Narrowing in on the temperature control has allowed ice-core scientists to use water isotopes to parse out temperature signals and shifts throughout time, hence the term "temperature-proxy" (Jouzel et al., 1997). Research on the water cycle and its connection to climate dynamics focuses on oxygen-18 and deuterium (and to a lesser extent, oxygen-17), the heavy isotopes of oxygen-16 and hydrogen (Dansgaard, 1964; Jouzel & Merlivat, 1984). Because heavier isotopes prefer to remain in their lowest energy states (e.g. liquid over gas), they preferentially precipitate out as atmospheric temperatures decrease, a process known as Rayleigh distillation (Sharp, 2017). Thus, warmer air preserves higher (less negative) values of oxygen-18 and deuterium while colder air exhibits lower (more negative) values (Dansgaard, 1964; Jouzel & Merlivat, 1984). The average abundance of oxygen and hydrogen isotopes are shown in Table 1 (Coplen et al., 2002; Sharp, 2017).

Isotope	Average terrestrial abundance (atom %)
^{16}O	99.7621
^{17}O	0.03790
^{18}O	0.20004
^{1}H	99.9844
D	0.01557

Table 1: Absolute abundance of stable oxygen and hydrogen atoms on the Earth

Isotope measurements are typically reported in terms of delta values (δ), which converts the ratio of heavy to light isotopes to the per-mil scale (‰) (Dansgaard, 1964). This research examined and reported the concentration of ^{18}O and D (sometimes referred to as ^{2}H) as a ratio of the heavy to light isotope in the sample as given by the relationship:

$$(1) \qquad R_x = \frac{^{18}O}{^{16}O} \; or \; R_x = \frac{D}{^{1}H}$$

The ratio is referenced against the known value of Vienna Standard Mean Ocean Water (VSMOW), with a value of 0‰, to obtain the amount of the heavy isotopes in relation to the global standard (Markle & Steig, 2022), given by equation 2 below, where R_x represents the measured ratio in the sample, and R_{std} is the ratio of VSMOW.

$$(2) \qquad \delta = \frac{R_x - R_{std}}{R_{std}}$$

Isotope values are reported in this way because it is considerably difficult to obtain the exact concentration of an isotope in a sample, but comparable easy to measure relative amounts (Tiwari et al.,

2015). δ^{18}O and δD are observed to behave very similarly, the relationship between the two given by a nearly linear slope, referred to as the Global Meteoric Water Line (GMWL) (Gat, 1996; Rozanski et al., 1993). Deviations from the nearly-linear relationship between δ^{18}O and δD is quantified by the parameter deuterium-excess (d_{xs}) and is widely used to examine correlations between isotope composition and air moisture behavior (Jouzel & Merlivat, 1984). Deuterium excess, shown in equation 3, is a metric that attempts to quantify the processes of kinetic fractionation. Typically, kinetic fractionation processes drive deviations from the GMWL slope. We will also refer to d_{ln} throughout this paper, which the non-linear definition for d_{xs}, and is a slightly more accurate representation of the relationship between δ^{18}O and δD (see equation 4) (Uemura et al. 2012; Markle et al. 2017; Markle & Steig, 2022). In equation 4, $\delta' = \ln(1 + \delta'_x)$, and the unitless coefficients A and B are defined as A = –28.5 and B = 8.47 (Uemura et al. 2012; Markle et al. 2017; Markle & Steig, 2022).

(3) $$d_{xs} = \delta D - 8 \times \delta^{18}O$$

(4) $$d_{ln} = \delta' D - (A \times (\delta'^{18}O)^2 + B \times \delta'^{18}O)$$

Stable Water Isotope Records from Ice Cores

Stable water isotopes can record signals of atmospheric conditions and post-depositional processes. Many ice core projects throughout Alaska and Canada have examined atmospheric circulation and temperature trends through interpretation of water isotope records. Water isotope data from ice cores within the Wrangell St-Elias Mountains, on Mt. Logan and the Eclipse Icefield, show that moisture sources to alpine glaciers differ based on site elevation (Zdanowicz et al., 2014). Higher elevation sites (Mt. Logan) interact with the free troposphere, and thus receive moisture from thousands of kilometers away that is reflective of large-scale atmospheric circulation trends. In contrast, lower elevation sites (Eclipse Icefield) interact with the lower troposphere and receive precipitation and moisture from local storms in the Gulf of Alaska and the northeast Pacific basin (Zdanowicz et al., 2014). In the Alaskan Arctic, ice core water isotope records from the McCall Glacier were used to explore ocean-atmosphere interactions. Klein et al. (2016) showed that high d_{xs} values are indicative of arid moisture derived from the Arctic Ocean where the source air parcel location is dominated by broader sea ice cover. Conversely, humid, moisture sources with relatively less sea ice from the Bering Sea are reflected in low d_{xs} values. From this project, precipitation at the McCall Glacier was shown to be sourced from increasingly sea ice-free water, effectively correlating water isotope records to atmospheric circulation patterns.

Post-depositional effects take place after snow has fallen in a region, and generally refer to concepts such as wind scour, sublimation, diffusion, fractionation during melt or meltwater refreezing and percolation, and snow metamorphism (Taylor et al., 2001; Tianming et al., 2020; Masson-Delmotte et al., 2008). Studies ranging from temperate glaciers in the Himalayas to the polar ice sheets of Antarctica and

Greenland report alterations of stable water isotope concentrations linked to various post-depositional processes. Such processes that potentially alter glacial geochemistry and impact the preservation of temperature signals have implications for water isotope thermometry and paleoclimatology in that they may alter the way in which temperature reconstructions are made and shift the signal interpretations from stable water isotopes (Moran & Moran, 2009; Pu et al., 2020; Wahl et al., 2021). Meltwater percolation research done by Taylor et al. (2001) found that isotope values become progressively less negative, or enriched in ^{18}O, as the snowpack experiences melt. Research in the Canadian Arctic found that during the melt season, isotopic modification is dominated by meltwater percolation, which is responsible for reducing the range of the seasonal signal and for isotopically enriching the ^{18}O measured in the snowpack (Moran & Moran, 2009). Meltwater studies from the Tibetan Plateau concluded that the melting process was responsible for isotopic enrichment of ^{18}O, though the exact quantity of change was uncertain (Pu et al., 2020). Though the above studies have determined that meltwater percolation has a homogenizing and enriching effect on ^{18}O and have suggested that meltwater refreezing could potentially cause fractionation, this question remains speculative and requires further research to determine the measurable extent of refreezing on fractionation. Accounting for post-depositional effects thought to alter the glacial isotope composition remains an open topic for ice-core analysis and water isotope geothermometry.

The Matthes-Llewellyn Ice Core

The JIRP research team drilled the Matthes-Llewelyn (ML) Ice Core on July 14, 2019 at the ice flow divide of the Matthes and Llewelyn Glaciers. An ice divide delineates the location where two glaciers are flowing away from a high point, or dome. The ice at a divide is primarily impacted by vertical compression, and not significantly altered by horizontal ice flow through the glacial depth. These characteristics make a divide a suitable location for an ice core, because the ice layers have not been deformed and preserve a chronological climate record that increases with depth (Martini et al., 2001). The ML Ice Core was drilled near the highest ice elevation on the icefield (58.85092˚N, 134.13038˚W, 1848 m.a.s.l) to a total depth of 294m. From ground penetrating radar (GPR) transects taken in July of 2019, it is estimated that the ice thickness at the drill site is between 350-450m deep (Seth Campbell, personal communication, March 6, 2023). The ML Ice Core was processed and sampled in the field at 50cm resolution, with samples temporarily stored and melted in quart-Ziploc bags, decanted into 100ml plastic Nalgene bottles, then pipetted into 5ml glass vials. At the University of Alaska Anchorage, the water isotope ratios ($\delta^{18}O$ and δD) of each sample were measured by Dr. Eric Klein with a cavity ring-down laser spectrometer, the Picarro L2130, which measures relative concentrations of isotopes based on laser absorption (*Picarro*, n.d.). Liquid measured on a Picarro L2130 have precision values of 0.025‰ for $\delta^{18}O$ and 0.1‰ for δD (*Picarro*, n.d.). All samples were measured in Fall and Winter 2019.

Initial analysis done by Bradley Markle and Eric Klein with the help of the JIRP staff revealed water isotope anomalies at and above the firn-ice transition within the upper 24.5 meters of the ML Ice Core. Firn is a solid with density and crystal formation between snow and ice (Martini et al., 2001). During the drilling of the ML Ice Core, a firn aquifer was reached just above the firn-ice transition. A firn aquifer is similar to a groundwater aquifer; liquid water pools in the loose pore spaces between snow crystals. The stable water isotope values of the ML Ice Core are plotted below in Figure 2 and illustrate the anomalous variability in water isotope values at and above the firn-ice transition at 24.5m.

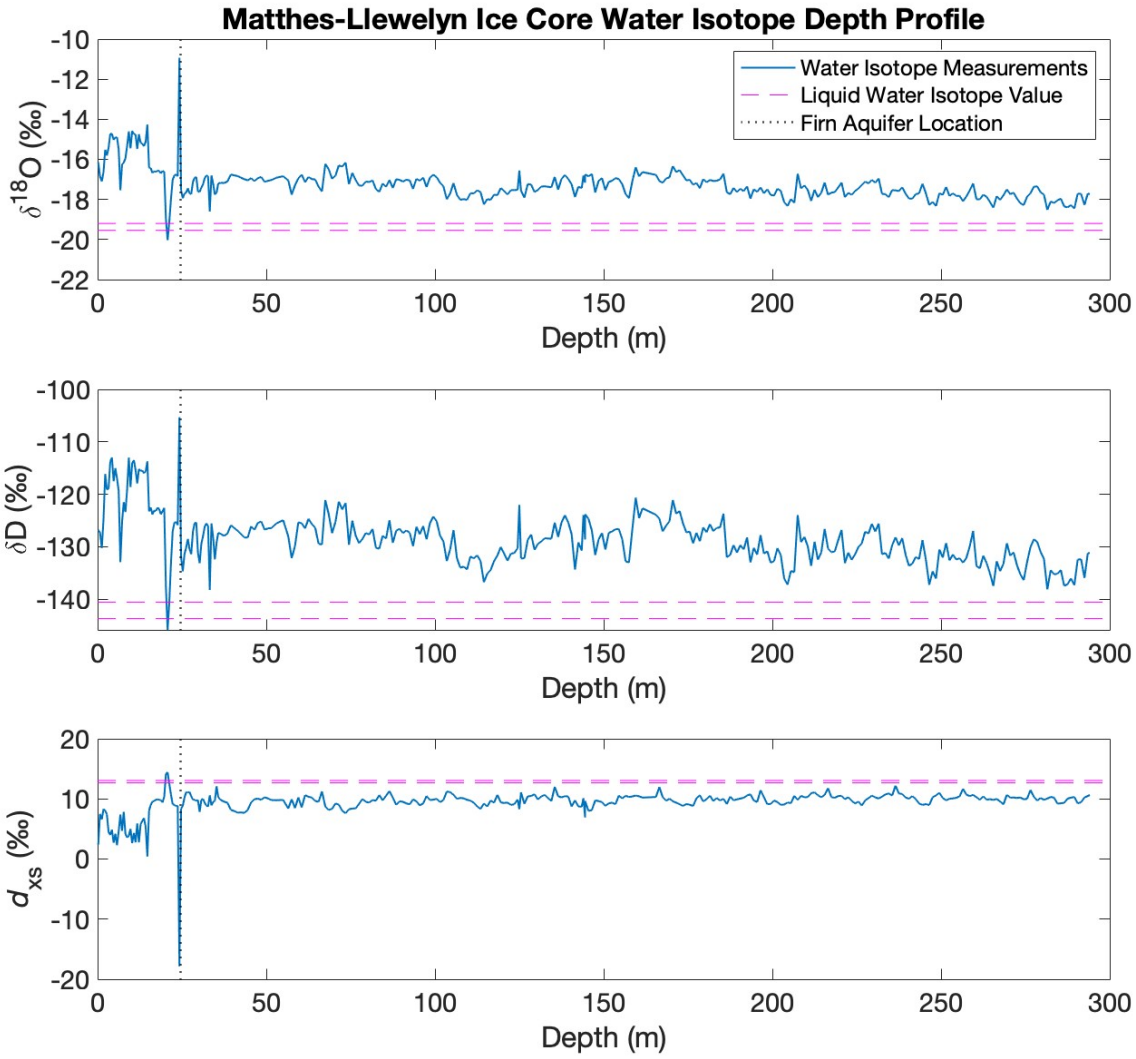

Figure 2: Stable water isotope data from the ML Ice Core plotted vs. depth from the surface. The surface of the ice is at 0m and the core bottom is at 294m. The location of the firn aquifer, i.e. the firn-ice transition, is indicated by the dotted black line, at 24.5m. Pink dashed lines indicate the water isotope values of liquid water sampled from the water table within the borehole, on two separate days of drilling (Bradley Markle and Eric Klein, unpublished data, personal communication).

The water isotope anomalies measured in the ice core are visible in the $\delta^{18}O$ and δD records and reinforced by the same variability in the d_{xs} relationship. The $\delta^{18}O$ and δD plots resemble one another because $\delta^{18}O$ and δD are linearly related at these latitudes, though the magnitudes of mass and relative abundance differ for $\delta^{18}O$ and δD. The most significant spikes in $\delta^{18}O$ and δD occur at 20.75m and 24.25m, above the firn-ice transition. Throughout the snow and firn (0-24.5m), the $\delta^{18}O$ and δD measurements are approximately 1.3‰ and 7.64‰ higher (less depleted in heavy isotopes) than the respective ice values. The d_{xs} values represent the relationship between $\delta^{18}O$ and δD and show a comparable shift above the firn-ice transition, with a decrease in mean d_{xs} values of approximately 3.23‰ relative to the mean ice d_{xs} (see Table 2). The firn aquifer liquid water table thickness was 4.78cm. Table 2 shows the mean and standard deviation $\delta^{18}O$, δD, and d_{xs} values for the snow/firn and glacial ice portions of the core. Row 1 excludes the visible spikes at 20.75m ($\delta^{18}O$ = –20.03‰, δD = –145.8‰), at 24.25m ($\delta^{18}O$ = –10.931‰, δD = –105.3‰), and at the liquid water table, while row 2 includes those values. Row 3 excludes any samples taken above 24.5m, to examine the water isotope distribution of the glacial ice only.

Sample Type	$\delta^{18}O$ mean (‰)	$\delta^{18}O$ sd	δD mean (‰)	δD sd	d_{xs} mean (‰)	d_{xs} sd
Firn (no anomalies)	–16.06	1.12	–121.72	6.56	6.75	3.02
Firn (w/ anomalies)	–16.04	1.43	–121.88	7.66	6.41	4.71
Water Table (liquid)	–19.37	—	–142.11	—	12.862	—
Ice	–17.41	0.47	–129.44	3.59	9.83	0.83

Table 2*:* Mean and standard deviation for firn, ice, and liquid water samples from the ML Ice Core.

Research Overview

This research aims to address the drivers of the water isotope anomalies in the top 24.5m of the core shown in Figure 2. The anomalies could be linked to three potential causes: shifts in the atmospheric water vapor pathway, changes in sea surface temperature at the moisture evaporation source, or post depositional effects of the meltwater in the firn aquifer. Big picture, the causes are either pre-depositional (before precipitation), or post-depositional (after precipitation). The ultimate research goal is to understand if there is a relationship between this variability and the presence of meltwater within the ice. Previous studies argue that meltwater infiltration in temperate glaciers leads to a wash-out of measured chemical markers, jeopardizes clear seasonal stratigraphy and geochemical signals, and compromises the scientific value of obtained data (Koerner, 1997, Neff et al., 2012, Schotterer et al., 2004). However,

ongoing research on Mt. Waddington has revealed that melt-impacted temperate glaciers can still preserve valuable isotope records because annual stratigraphy is still visible when meltwater infiltration through the ice is superseded by snow accumulation rates (Neff et al., 2012). Specific to the ML Ice Core, we believe that the water isotope signal below the firn-ice transition is generally preserved (see Fig. 2). However, the extent, if at all, to which the firn aquifer has impacted the upper snow and firn regions of the ice core is still unclear.

To investigate the question of pre- versus post-depositional drivers, we first approximated the depth-age relationship for the 2019 Matthes-Llewellyn Ice Core using the Dansgaard-Johnson flow model. Understanding the age of the ice throughout the ice core depth allowed us to contextualize the timing of potential climate conditions causing the water isotope anomalies. Next, we input the ML Ice Core water isotope data into Simple Water Isotope Model (SWIM) to examine the reconstructed absolute evaporation and precipitation temperatures for the snow reaching the Juneau Icefield. SWIM outputs suggested an evaporative temperature decline over approximately the past ten years. We pursued this possibility by comparing National Center for Environmental Prediction (NCEP) SST reanalysis data to the National Oceanic and Atmospheric Administration (NOAA) Hybrid Single-Particle Lagrangian Integrated Trajectory (HySPLIT) modeled air parcel back-trajectories for the years correlating to the firn-ice transition to understand whether climate conditions are linked to the water isotope anomalies. Last, we analyzed water isotope data from snow pits collected in 2021 on the Juneau Icefield to begin preliminarily exploring the effects of meltwater infiltration on water isotope behavior. We ask if the water isotope anomalies present at and above the firn-ice transition are coincidentally at the same depth of the observed firn aquifer, i.e. caused by climate conditions, or if the data variability is driven by post-depositional processes involving the presence of meltwater. More so, we consider if it is possible to disentangle the two options.

Depth-Age Modelling

Methods

Ice core age dating generally relies upon a variety of empirical and theoretical methods including ice core comparison against marine sediment cores, volcanic ash isotopic identification, and annual layer counting through dust and accumulation markers (Lemieux-Dudon et al., 2010; Nardin et al., 2021). Dating methods are constantly improving and vary by chemical species, and are adjusted according to the type of glacier and ice conditions at the drill site. Polar ice cores (in Greenland and Antarctica) are often dated through a combination of glaciological modeling and gas measurements matched to global markers chronologically constrained by other geological sources (Lemieux-Dudon et al., 2010). Recent studies on high alpine glaciers have used methods such as radiocarbon dating from dissolved organic carbon, annual layer counting, and nuclear fallout plutonium concentration signals in addition to ice flow modeling (Fang et al., 2021; Klein et al., 2016; Shao et al., 2020).

In the case of the ML Ice Core, because stable water isotope ratios were the only species measured throughout ice depth, the usual ice core dating methods were not applicable. Thus, to constrain the age of the ML Ice Core, this project utilized an ice flow model based upon the fundamentals of glacial physics. Specifically, we used the Lliboutry (1979) parameterization of the Dansgaard-Johnson (DJ) flow model, provided by TJ Fudge at The University of Washington (personal communication, January 15, 2023). The DJ model builds on an earlier ice flow model written by Nye (1957), which uses equation (5) to approximate ice age where h denotes the depth to bedrock (m), b is the accumulation rate in meters of ice equivalent, and z is the ice core depth.

(5) $$\text{age} = \frac{h}{b} ln(\frac{1}{1-\frac{z}{h}})$$

With this basis, the DJ model calculates the age of a layer (t) through equations (6) and (7) by incorporating the initial annual layer ice thickness (λ_H), reduced annual layer ice thickness (λ), annual layer ice thickness at $y=h$ (λ_h), the present height above the bedrock (y), initial height above bedrock (H), and unit of time (τ). In equation (7), t_h denotes the age of the ice layer at $y=h$ from equation (6) (Dansgaard & Johnsen, 1969).

(6) $$t = -\frac{h\tau}{2\lambda_h} \ln(\frac{2y-h}{2H-h}) \qquad \text{for } h \leq y \geq H$$

(7) $$t - t_h = \frac{(2H-h)\tau}{\lambda_h}(\frac{h}{y} - 1) \quad \text{for } 0 \leq y \geq h$$

The Lliboutry parameterized DJ model consists of two functions. The first uses the DJ model to calculate a depth age scale and the second adjusts the DJ model to account for basal melt. To do so, the overall parameterized model uses a defined time step, set to a range of 0-10,000 years in increments of 10 years. With the time step established, the DJ model utilizes the ice accumulation rate, modern ice

thickness, ice flow parameter, basal melt rate, and glacial sliding fraction to output the approximate age scale of the given ice core. The model also assumes ice-equivalent depths; therefore, the densities and thicknesses of the upper ice core samples (snow and firn) were converted using equation (8), where the ice-equivalent sample length, l_i is found by multiplying sample density (ρ_s) by the quotient of sample length (l_s) and ice density (ρ_i).

(8) $l_i = \rho_s(\frac{l_s}{\rho_i})$, l_s = bottom $\text{depth}_{\text{sample}}$ - top $\text{depth}_{\text{sample}}$

From the approximate density profile of the ice core, new depth values for the top and bottom depth of each core segment were generated using equation (8), where sample length is the difference between the bottom and top depth of an ice core segment. The top 5m of the ML Ice Core were assigned an assumed snow density of 0.60kg/m^3, based on the mean snow density from six shallow snow cores, ranging in depth from 2.02 to 7.5m, drilled during the 2021 field season. From a depth of 5m to the ice transition at 24.5m, the snow depth was calculated by assuming a linear density increase from 0.60g/cm^3 to 0.917g/cm^3, the average glacial ice density (Anderson & Anderson, 2010). This is a fair assumption to make because as glaciers increase in depth, the snow is gradually compressed into firn and ice, thus the material density also increases (Anderson & Anderson, 2010; Martini et al., 2001).

After adjusting for ice density, the following parameters were altered to test the model sensitivity and produce an approximate depth-age relationship throughout ice depth: seasonal accumulation rate (meters of ice equivalent), ice flow mechanism, and total ice thickness (m). First, accumulation rate was estimated at 2m ice-equivalent/year, then given random variability of ±0.5m, to simulate random seasonal variability, an estimate based on average annual snow accumulation on the Juneau Icefield (Chris McNeil, personal communication**)**. Next, accumulation rate was held constant at 2m/year, while four different ice flow parameters were tested. Assuming that the ice at the drill site flows according to flank flow, meaning the drill site is not directly at the ice divide, values between four and ten are reasonable inputs to the model (Lliboutry, 1979; Parrenin et al., 2007). Last, the ice thickness parameter was adjusted, while the accumulation rate (2m/yr) and ice flow parameters (h=10) were kept constant. Because the GPR transects at the ice divide did not produce clear images of the entire ice stratigraphy, the total ice thickness at the drill site is uncertain. We estimate the thickness to be between 450m and 350m, and plot three outputs of the model, in 50m increments (450m, 400m, and 350m).

Depth-Age Modeling Results

The first step in understanding the ML Ice Core was to determine an approximate depth-age relationship so that subsequent analysis could be chronologically contextualized. Although estimating ice age was difficult for the ML Ice Core due to the limited scope of available data, we applied the Lliboutry parameterization of the DJ flow model by using best estimates of model inputs. The DJ ice flow model was applied to the ML Ice Core, with three parameters adjusted: annual accumulation, ice flow factor, and total ice thickness. Adjusting the accumulation to account for probable random seasonal variability produces an age range for the ice at the firn-ice transition and total core age range of 10.34yrs ± 3 (1 SD) and ~256-305 years old, respectively. Within the ice flow factor, four different parameters that assume flank flow conditions at the drill site were adjusted (h=0.5, h=1, h=4, h=10). After this testing, the firn-ice transition was estimated at an age of 10 years and the total core age range landed between 280 and 455 years. Next, three ice thickness values that bracket the firn-ice transition age at ~10yrs were tested (H=350m, H=400m, H=450m), which estimated the total ice core age to range from 250 to 360ya. Figure 3 shows the results of the sensitivity testing. Figure 4 displays the firn-ice transition age estimates with all adjusted parameters layered on top of each other. As seen by the overlap of all tested parameters in Figure 4, accumulation rate variability had the largest influence on the firn-ice transition age and the smallest effect on the bottom-depth age with respect to the flow parameter and ice thickness. Additionally, the flow parameter values significantly altered the total core age estimate. Flow parameter values ranging from h=0.5 to h=10 were tested, but $4<h<10$ are much more likely scenarios at this drill site because they are reflective of flank flow ice conditions observed on the icefield. For sake of streamlining further analysis, the firn-ice transition will be estimated at 10ya, which correlates to the year 2009. Figure 5 displays the ML Ice Core water isotope values against the estimated ice core age profile. Age is displayed from present (left) to past (right), although some studies present time in the reverse (Clifford et al., 2019; Klein et al, 2016; Nardin et al., 2021). Although the ice-equivalent depth used for depth-age approximations is 19.2m (Figure 4), subsequent sections will refer to the sample depth of the firn-ice transition (24.5m). Determining the firn-ice transition age allowed for a deeper examination of the climatological drivers of the anomaly because we were able to narrow the focus of recent-past climate trends to the approximate year.

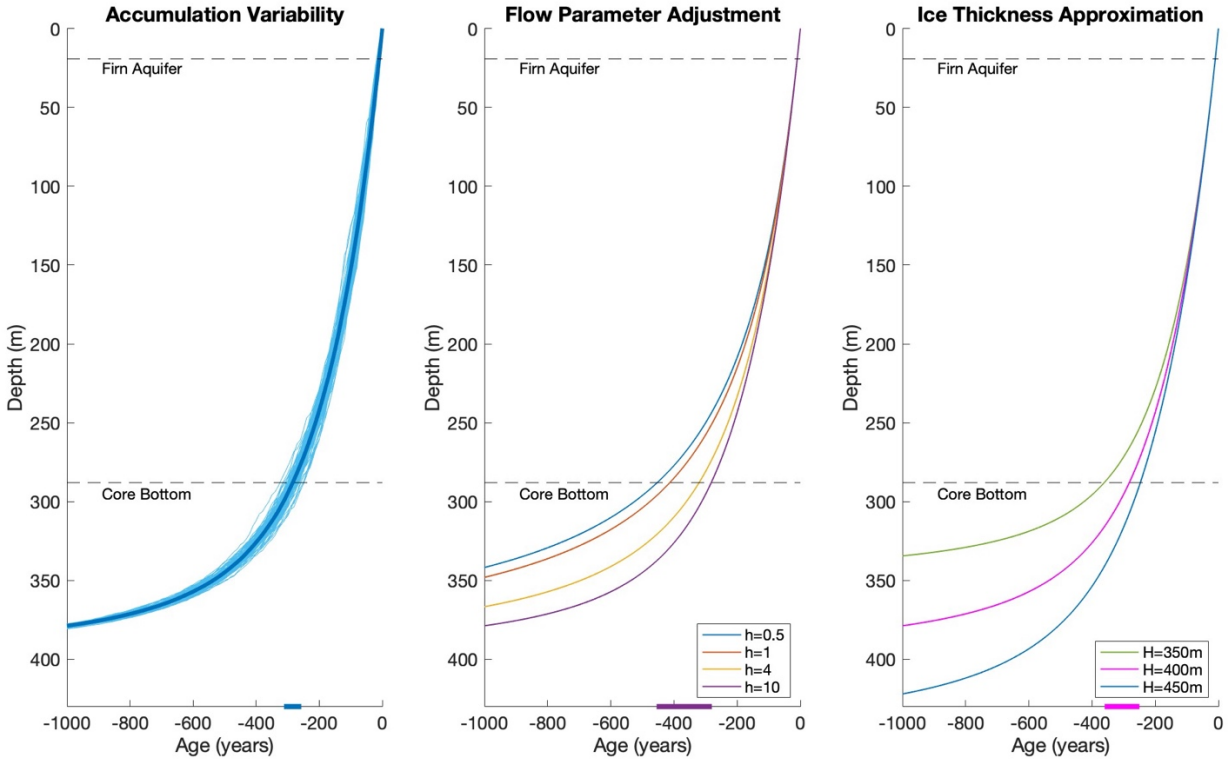

Figure 3: Total modeled ice core depth-age relationship. Depth increases downwards from the surface (0) to the estimated bedrock depth (350-450m). The colored bars on each x-axis represent the total core depth for each parameter. The bottom depth age of the core is estimated between 250 and 455 years, taking all tests into account.

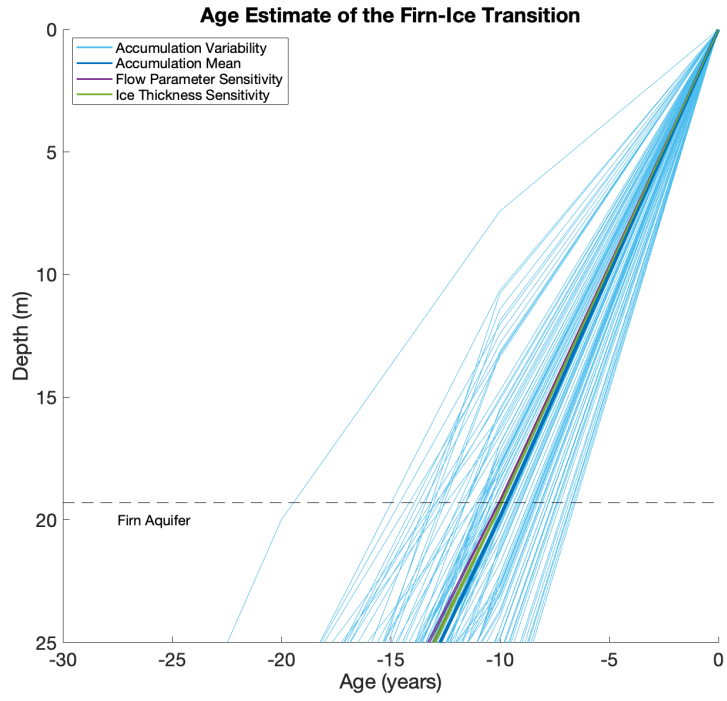

Figure 4: Estimated depth-age relationship for the upper 24.5m of the ML Ice Core using the DJ model. Accumulation rate, flow parameter, and total ice thickness were adjusted to test model sensitivity. All lines overlap with the exception of accumulation variability, which has the largest effect on firn-ice transition age estimates.

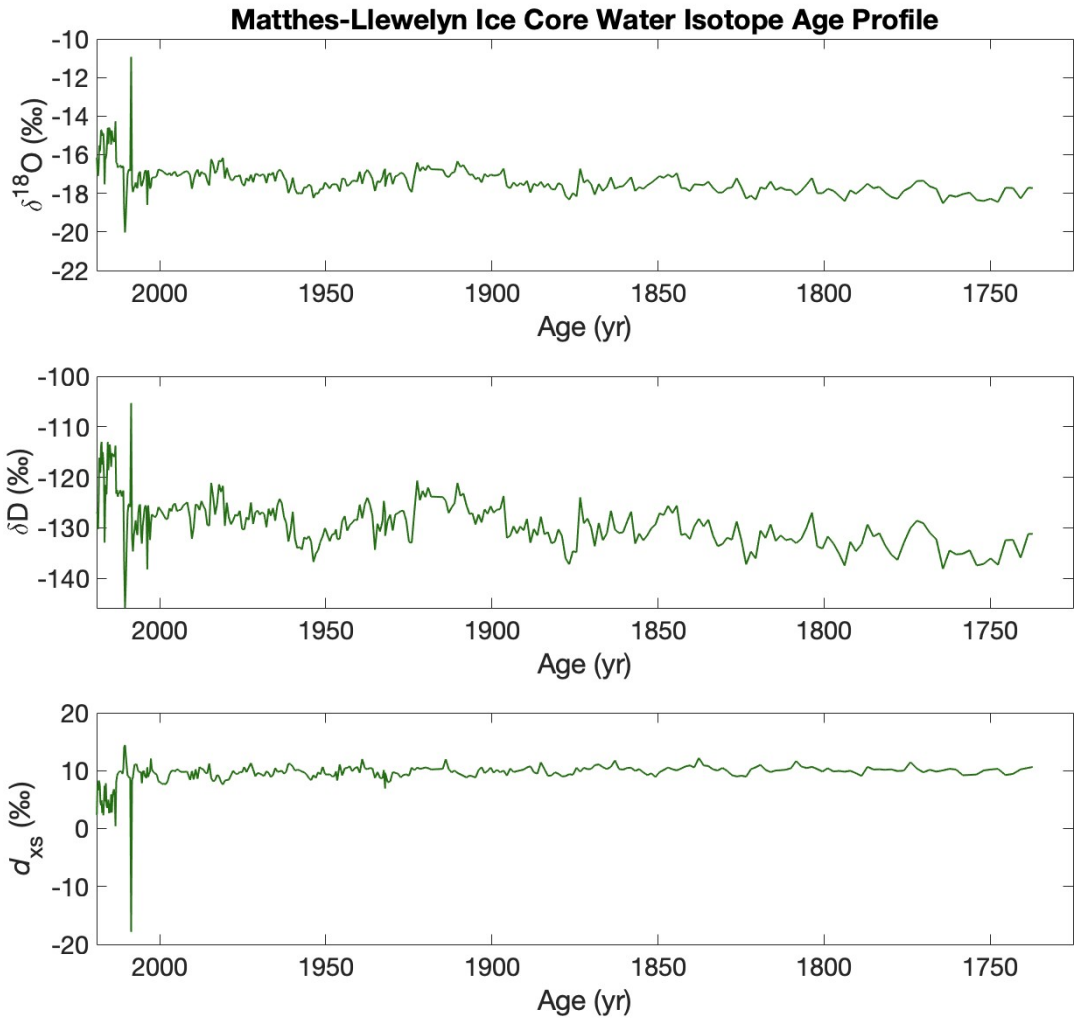

Figure 3: ML Ice Core water isotope values plotted against the estimated age of the ice core. Age is estimated above through sensitivity testing of the DJ flow model. The age scale represented in this figure is based on adjustments to the DJ model that assume annual accumulation of 2m/yr, a flank flow parameter of h=10, and total ice thickness of H=400m. Time has been represented from modern day (left) to past (right) for sake of comparison ease to Figures 2 and 8.

Water Isotope SWIM Modeling

Methods

Using the depth-age approximations allowed for a narrower constraint on the water isotope anomalies present at 24.5m in the ML ice core. We used the Simple Water Isotope Model (SWIM) to the Matthes-Llewelyn Ice Core water isotope data to examine atmospheric and site temperature trends (Markle & Steig, 2022). The SWIM is a Rayleigh type distillation model that represents the processes of evaporation and moisture transport and calculates the fractionation of water isotopes along transport paths. The model can be inverted to reconstruct temperature for measured water isotope ratios of precipitation. To do this, we first, prescribe a set of initial evaporation and final condensation air temperatures that are characteristic of the ice core drill site, derived from general site knowledge and JIF temperature records (Baker et al., 2019). Second, the model uses those input temperatures in conjunction with modern climate relationships of air temperature to sea surface temperature (SST) and relative humidity (RH) to predict starting values for SST and RH for likely vapor moisture sources. Third, SWIM then uses numerical expressions that describe the processes of evaporation and Rayleigh distillation, incorporating condensation along a moisture gradient and calculates fractionation. The result of this step is a matrix of all possible $\delta^{18}O$ and δD values for the initial evaporation and condensation temperatures. Finally, SWIM inverts this results matrix to create tables of starting and ending temperatures as functions of modeled water isotope values ($\delta^{18}O$ and d_{ln}) of final precipitation. Measured water isotope values from snow and ice samples can be used to determine the initial evaporation temperatures and final condensation temperatures for the given unique pairs of isotopes. $\delta^{18}O$ and d_{ln} are used to reconstruct these absolute temperatures because they are best paired. For the work described in this paper, we chose starting and ending temperature ranges that adequately pertain to the JIF (Baker et al., 2019), setting input site (final) temperatures between –40˚C and +15˚C, and source (initial) temperatures between 2˚C and 28˚C. Ultimately, we used SWIM to reconstruct evaporation source temperature (T_{evap}), condensation temperature (T_{cond}), and surface temperature ($T_{surface}$) from the water isotopes measurement in the ML Ice Core, to examine potential atmospheric conditions driving the shift in water isotope values.

SWIM Model Results

The Simple Water Isotope Model (SWIM) was used to output temperature reconstructions for the given ML Ice Core water isotope values. For the parameters that the model was set to, SWIM reconstructed the evaporation source temperature (T_{evap}), condensation temperature (T_{cond}), and surface temperature ($T_{surface}$) for the precipitation at the ML Ice Core drill site. Figure 6 shows the initial output of the matrix of all possible $\delta^{18}O$ and δD values for the initial evaporation and condensation temperatures, and Figure 7 displays the inversion of the SWIM model used to reconstruct absolute temperature for the

ML Ice Core. Evaporation source temperature refers to the temperature that the water vapor originated at over the Pacific Ocean, where the majority of precipitation on the Juneau Icefield is derived from. Condensation temperature describes the temperature weighted vertical profile of precipitation at the drill site (Markle & Steig, 2022). Surface temperatures generally related to condensation temperature by a linear slope between 0.62 and 0.67 ˚C˚C^{-1} and thus should show similar patterns of variability to the condensation temperatures with different absolute magnitudes (Markle & Steig, 2022). The results of SWIM are shown below in Figure 8 and Table 3 and indicate that the evaporation source temperature of the precipitation arriving at the Juneau Icefield in the past twenty years potentially shifted down by an average of 5˚C. The model did not show significant change in condensation temperature or surface temperature.

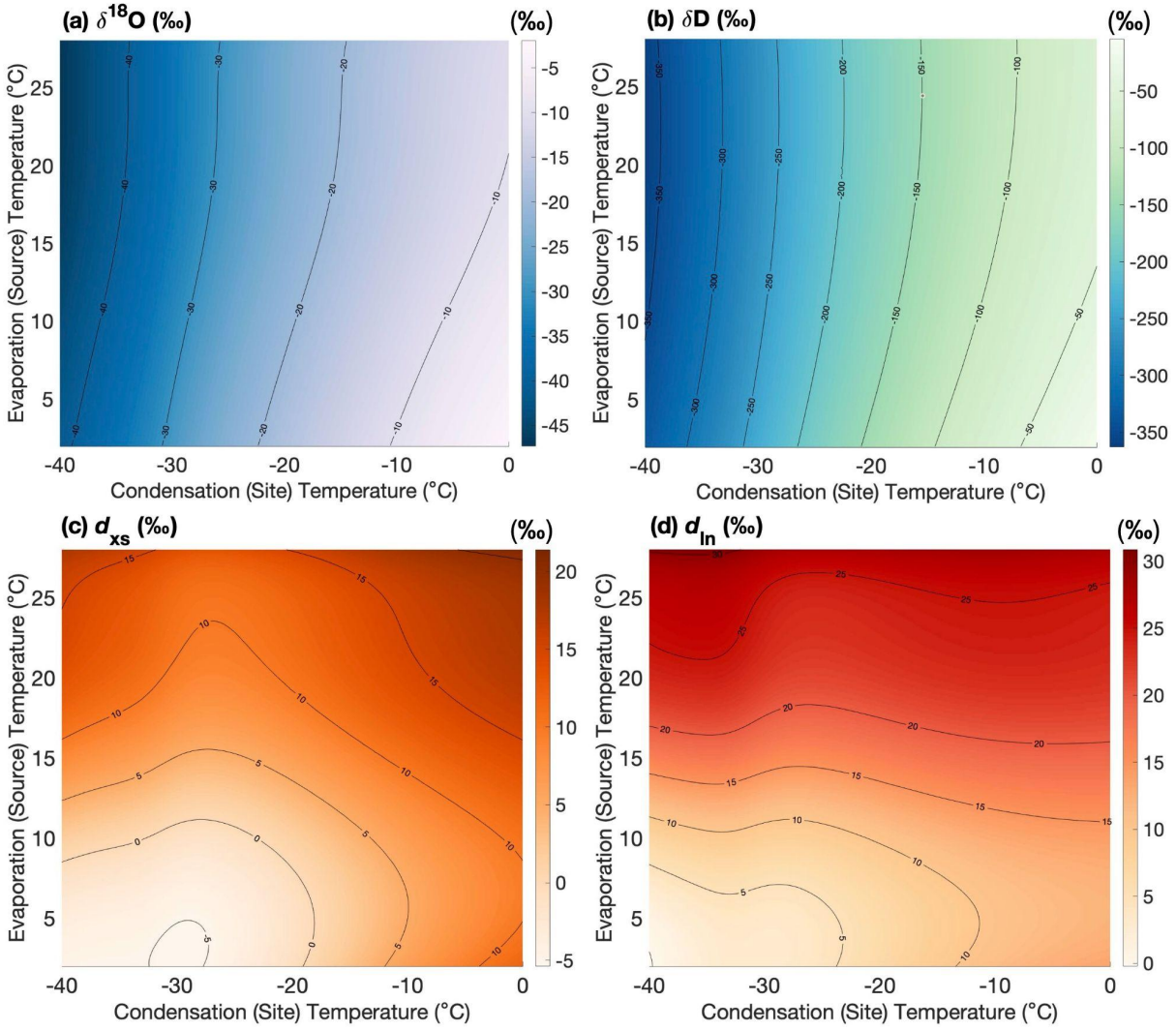

Figure 4: Initial water isotope configurations for all possible given ranges of starting evaporation (2˚C to 28˚C) and condensation (–40˚C to +15˚C) temperatures. Color gradients represent the water isotope precipitation values calculated by SWIM.

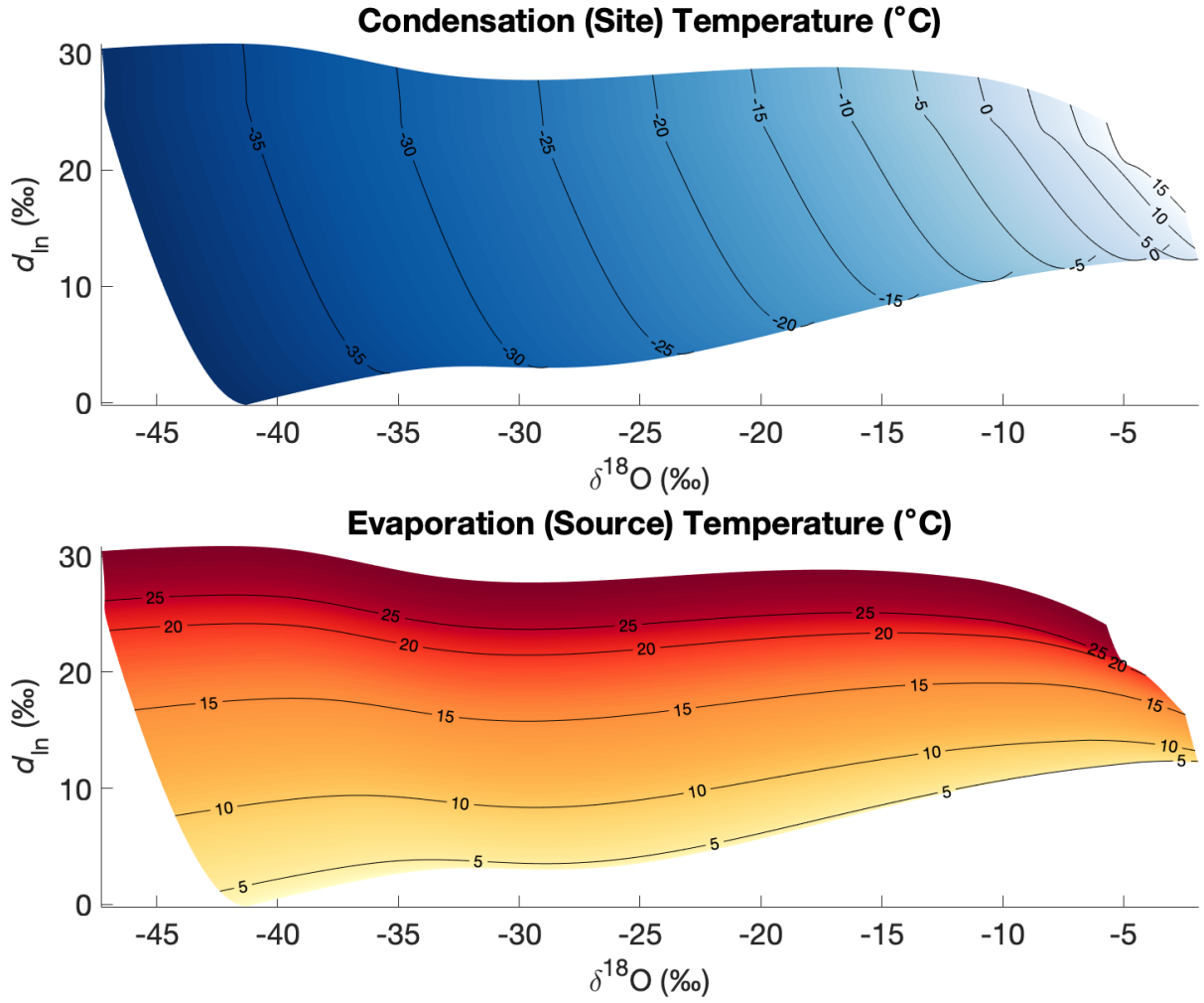

Figure 5: SWIM results of model inversion using outputs from modeled isotope relationships to constrain possible condensation and evaporation temperatures specific to the ML Ice Core. We display $\delta^{18}O$ as a function of d_{ln} because it more accurately depicts moisture source than d_{xs}.

Temp. Output	Mean Temp (˚C) (Firn/Snow) Depth < 24.5m	Standard Deviation Depth < 24.5m	Mean Temp (˚C) (Ice) Depth > 24.5m	Standard Deviation Depth > 24.5m
T_{evap}	10.1552	2.2770	15.5244	0.8866
T_{cond}	–13.5776	0.7875	–13.4629	0.5094
$T_{surface}$	–7.7936	1.1413	–7.6274	0.7382

Table 3: Empirical SWIM results of T_{evap}, T_{cond}, and $T_{surface}$ for the ML Ice Core water isotope data.

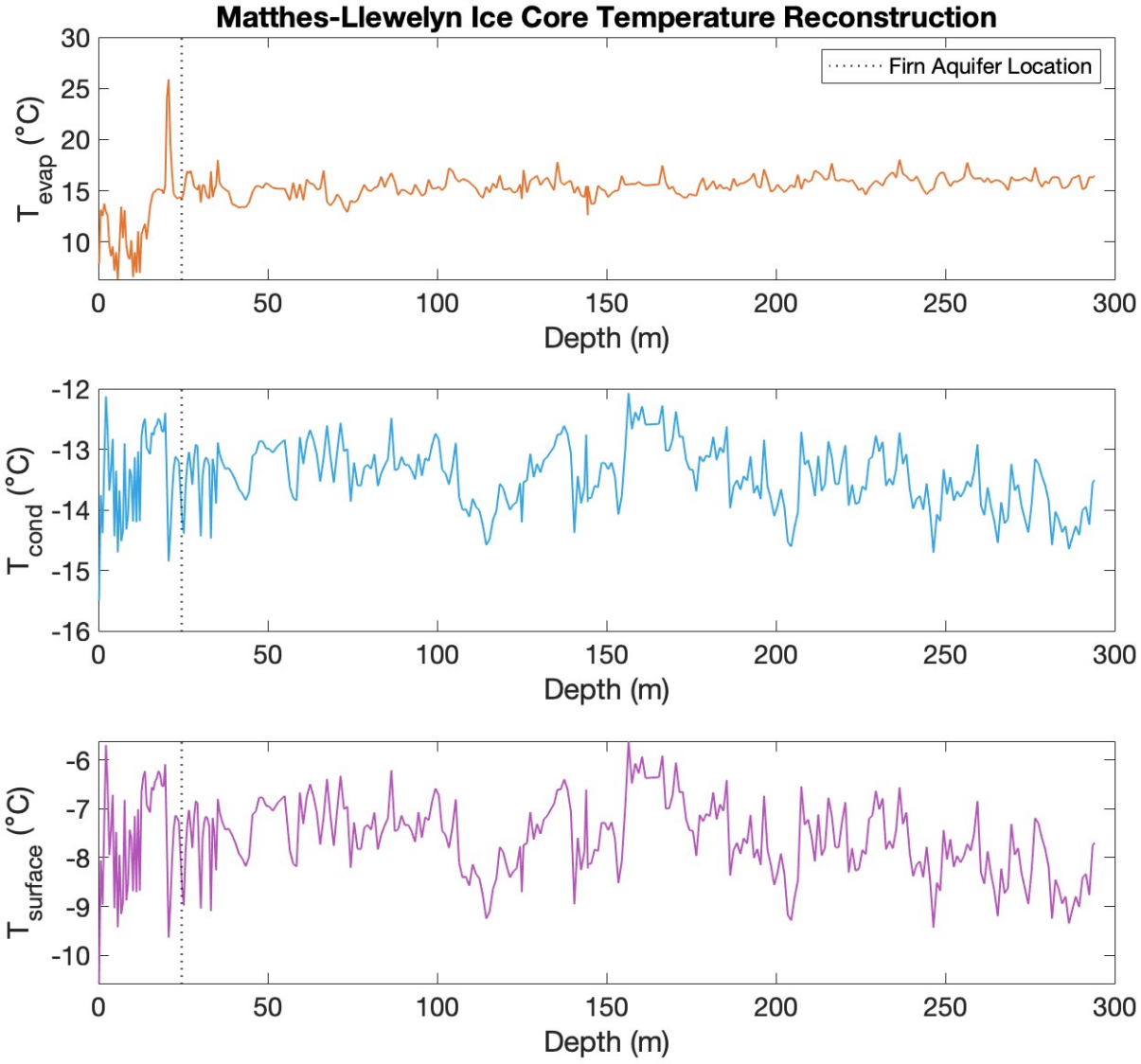

Figure 6: SWIM temperature reconstructions of T_{evap}, T_{cond}, and $T_{surface}$ for the given ML Ice Core water isotope values.

Sea Surface Temperature Reanalysis and HySPLIT Back-Trajectory Modeling

Methods

To explore the effects of sea surface temperature (SST) shifts on the evaporative source conditions (estimated by SWIM) potentially driving the anomalous water isotope signal, we mapped SST average temperatures for the past twenty years and compared the temperature anomalies to air parcel transport pathways generated by the National Oceanic and Atmospheric Administration (NOAA) Hybrid Single-Particle Lagrangian Integrated Trajectory (HySPLIT) model (Draxler & Hess, 1998). Because the majority of snowfall accumulation on the Juneau Icefield occurs in the winter months (October-May), National Center for Environmental Prediction (NCEP) reanalysis SST data available through the NOAA Physical Sciences Laboratory was plotted for these months averaged over the year ranges of 2000-2010 and 2010-2020. These intervals were chosen because the best estimate of the age of the ice at the firn-ice transition was estimated at approximately 10yrs. The difference between the 10-year average SST outputs was calculated to display the SST anomalies during this time period, with the goal of contextualizing SWIM outputs. Additionally, we plotted long-term mean sea surface temperatures (1990-2020) to compare HySPLIT back-trajectories to absolute SST.

The HySPLIT model is used to understand storm trajectories, climatic conditions, and atmospheric transport of air parcels when given certain parameters: site location, height above ground level, and trajectory time (Draxler & Hess, 1998). This study utilized HySPLIT to narrow in on the water isotope anomalies by examining the average air parcel trajectories for the year prior (2008) to and after (2010) the age-dated firn-ice transition, as estimated by the depth-age approximation (see Figs. 3, 4, and 5). Through a combination of Lagrangian and Elerian calculations, HySPLIT is able to combine multiple meteorological datasets to output the most precise trajectory. Specifically, the Lagrangian equations applied are useful for advection and diffusion calculations of a "moving frame of reference", whereas the Eulerian equations are employed in order to evaluate the concentration of air pollutants in a "fixed three-dimensional grid" (Stein et al., 2015). To describe the dispersion of air parcels through a given atmospheric pathway and more accurately plot a specific trajectory, HySPLIT utilizes equations (9) and (10), where U' and W' represent the turbulent velocity component, X_{mean} and Z_{mean} mark the final horizontal and vertical positions of the air parcel, and t denotes temperature.

$$X_{final}(t + \Delta t) = X_{mean}(t + \Delta t) + U'(t + \Delta t)\,\Delta t \quad (9)$$

$$Z_{final}(t + \Delta t) = Z_{mean}(t + \Delta t) + W'(t + \Delta t)\,\Delta t \quad (10)$$

The age of the ice at the firn-ice transition was estimated at approximately 10 years, meaning it dates to 2009. Given monthly global NCEP reanalysis data, ten-day (240hr) HySPLIT back-trajectories were run for each day of the two years (2008 and 2010) on either side of the firn-ice transition to examine the validity of the SWIM Model evaporation source temperature estimates. Air parcel initial starting

conditions were set at 1500m above ground level (m.a.g.l), to ideally be able to locate the original evaporation source. 1500m.a.g.l. is a common initial altitude at which HySPLIT is run because it is generally a sufficient height at which to sample the free troposphere, the atmospheric region of most large-scale movement of storms and general atmospheric circulation (Brönnimann, 2020; Markle et al., 2012; Winski et al., 2018). HySPLIT outputs for the daily back-trajectories were clustered into five transport pathways per year, with the mean of each year displayed as one cluster of all back-trajectories. Cluster analysis of daily back-trajectories allows for concise visualization of typical air parcel transport pathways for precipitation arriving at the ML Ice Core drill site on the Juneau Icefield (Dorling et al., 1992; Markle et al, 2012). Previous studies have found that the use of NCEP reanalysis in high latitude HySPLIT reconstructions compared to European Center for Medium Range Weather Forecast 40-year (ERA-40) reanalysis introduced "relative horizontal transport deviations (RHTD) of 30–40% of the trajectory length" (Markle et al., 2012, p. 4; Harris et al., 2005). Regardless, NCEP data is used in this study because has shown to have strong correlation to ground-truthed weather station data post 1979, and our research only extends back to 1990 (Bromwich & Fogt, 2004, Markle et al., 2012).

HySPLIT Air Parcel Back-Trajectories and SST Reconstructions

HySPLIT air parcel back-trajectory models for 2008 and 2010 and NCEP/NOAA mean sea surface temperature (SST) reconstructions for the years before and after the firn-ice transition (2000-2020) do not show significant temperature shifts. The majority of the precipitation reaching the Juneau Icefield, as estimated from HySPLIT back-trajectories, originates from the Pacific Basin above ~40˚N, with a smaller portion of the precipitation sourced from the Bering Sea and Arctic Ocean (>70˚N) (see Fig. 9). HySPLIT runs were set to cluster 2008 and 2010 data because the firn-ice transition was dated to 2009; thus, the goal was to gain insight on atmospheric shifts that could potentially lead to the water isotope data anomalies. Figure 9 below shows the mean October-May SST reconstructions from global NCEP reanalysis data, plotted through the NOAA Physical Sciences Laboratory, along with the HySPLIT back-trajectories for 2008 and 2010. In panels b) and c), trajectory line-thickness is proportional to the amount of days in each cluster per year (see Table 4).

The months of October through May for the years 2000-2020 best constrain winter precipitation on the Juneau Icefield based on the firn-ice transition age approximation (10.34yrs ± 2.99). The mean SST for the winter precipitation months in the Northern Pacific and Arctic Ocean range between –2˚C to +25˚C (see Fig. 9b and 9c), though the majority of water vapor transport to the Juneau Icefield derives from oceans with SSTs between –2˚C and +15˚C. Extreme cold values (below –2˚C) in the SST plots are reflective of sea ice cover, not liquid sea-water temperature. In the Pacific Basin, temperatures shifted by 0.5˚C colder to <1˚C warmer, near the coast of continental North America. In the Chukchi Sea between

northern Alaska and Russia and northern regions of the Arctic Ocean, SST cooled by a maximum of –3.5˚C and warmed by +3.5˚C, though these extremes are only represented in small pockets of the region. For the most part, the Arctic Ocean warmed by 1-2˚C from 2000-2020, and the Pacific Basin remained steady between –0.5˚C and +0.5˚C of temperature change.

Cluster Number	2008 Percentage (%)	2010 Percentage (%)
1	4	21
2	25	19
3	33	32
4	17	21
5	21	5

Table 4: HySPLIT back-trajectory outputs, as a percentage per cluster per starting location.

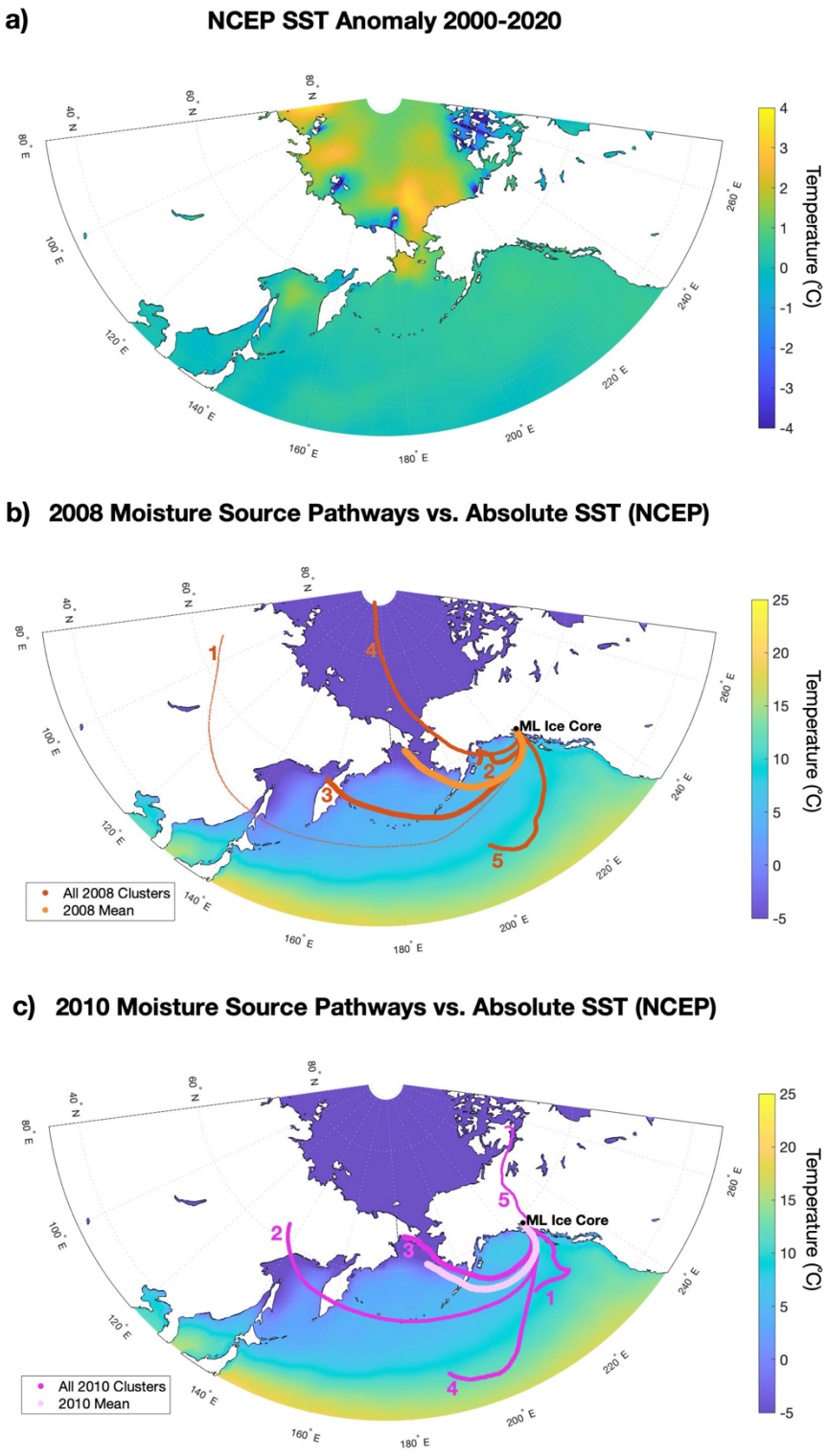

Figure 7: SST anomalies (a) as a difference between the 2010-2020 mean and 2000-2010 mean. 2008 (b) and 2010 (c) HySPLIT clusters on the long term mean absolute SST from 1990-2020, respectively. Data provided by the NOAA/ESRL Physical Sciences Laboratory, Boulder Colorado, http://psl.noaa.gov/

2021 JIRP Analysis

To add spatial context to the ice core, this research utilized quantitative analysis of snow and ice samples collected during the 2021 field season across the Juneau Ice Field (JIF). Samples were collected in three main forms shallow snow cores, snow pits, and surface transects (see Table 5). Figure 10 provides a map of these 2021 sample site locations. Sample group one consisted of six shallow snow cores ranging in depth from ~2m to 7.5m, with 5cm samples collected every 25cm (0.25m) from the snow surface. The snow cores were obtained with a hand-held drill provided by Seth Campbell at the University of Maine (Kovacs Mark II coring system, *Kovacs Enterprise*. n.d.). Sample group two included data from ten snow pits sampled every 50cm (0.50m) from the surface to depths ranging from 3.15m to 5.2m to examine annual snow accumulation and seasonal trends (Pelto et al., 2008). Sample group three consisted of six surface transects ranging from approximately 4km to 12km in length, with snow sampled at 500m intervals to a depth of 10cm (0.10m) below the surface, sampling glacial cross-sections and parallel-flow transects. 2021 samples in all three groups were collected at elevations from 959 to 2031 meters above sea level (m.a.s.l.) between early June and late July. Snow was packaged in quart-Ziploc bags then transferred to plastic or glass vials before air transit. In total, more than 350 samples were shipped from the JIF to the Stable Isotope Lab at the Institute of Arctic and Alpine Research at the University of Colorado Boulder.

Sample Group	Sampling Resolution (m)	Min Bottom Depth (m)	Max Bottom Depth (m)	Number per Group	Samples Collected
Shallow Core	0.25	2.05	7.53	6	131
Snow Pit	0.50	3.15	5.20	10	142
Surface Transect	0.10	0.10	0.10	6	84
Other	N/A	N/A	N/A	2	2
Total				24	359

Table 5: 2021 snow and firn samples collected across the JIF. Sampling resolution describes the frequency of samples taken per depth in the snowpack. The minimum and maximum bottom depth that shallow cores and snow pits reached is indicated by the respective columns.

I measured the water isotope composition of all 2021 samples at the Stable Isotope Laboratory using a Picarro L2130 in Fall 2021 (*Picarro*, n.d.). 40 samples were measured at a time, calibrated by three standards that bracket the samples between low and high known values, with one standard falling in the middle of the range for more accurate comparison. Samples were corrected for naturally occurring drift from the actual value using the known standard values. Liquid measured on a Picarro L2130 have precision values of 0.025‰ for $\delta^{18}O$ and 0.1‰ for δD (*Picarro*, n.d.).

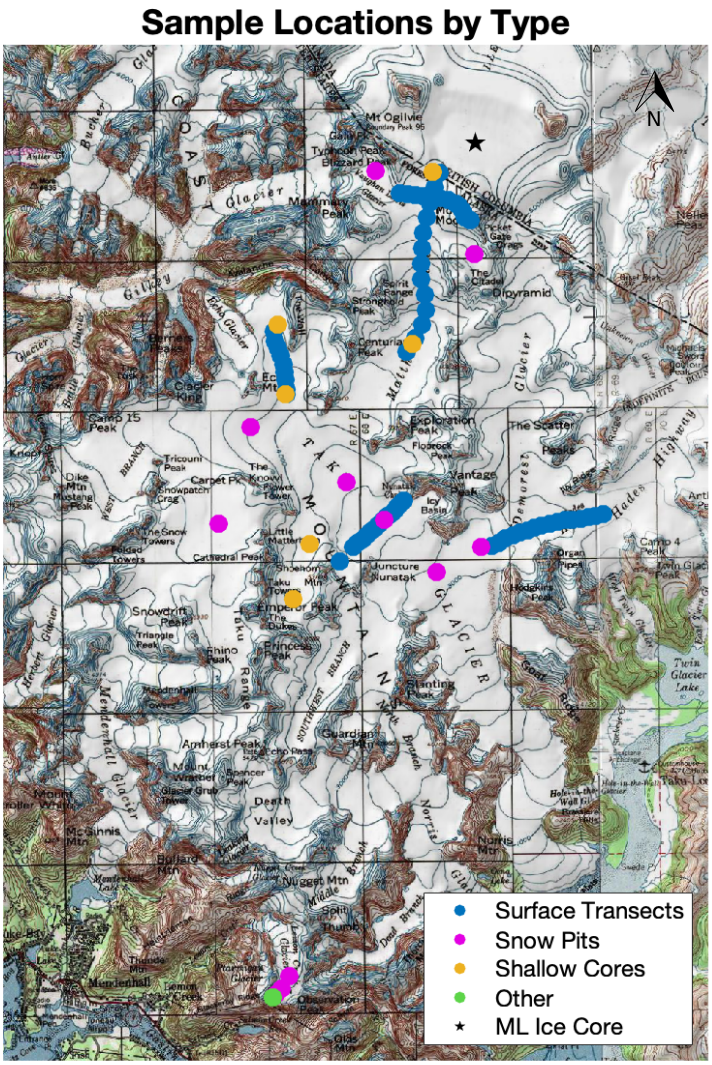

Figure 8: Map of 2021 data collection locations and 2019 ML Ice Core location. 2021 sample types are categorized into surface transects, snow pits, shallow cores, and other (rain & surface lake samples).

Central to this research is the question of meltwater impact on temperate glacial ice, specifically in the context of post-depositional effects on water isotope composition. To examine this further, we preliminarily analyzed the water isotope values from ice lenses sampled in the ten snow pits across the icefield were compared to snow samples from the same snow pits, across all sampled depths. The following null and alternative hypotheses were tested for $\delta^{18}O$, δD, and d_{xs}:

H_0 = the mean (μ) snow pit ice lens and snow sample ($\delta^{18}O$, δD, and d_{xs}) data are equivalent

$$\mu_{\text{ice lens}} = \mu_{\text{snow}}$$

H_a = the mean snow pit ice lens and snow sample ($\delta^{18}O$, δD, and d_{xs}) data are not equivalent

$$\mu_{\text{ice lens}} \neq \mu_{\text{snow}}$$

Samples were tested for normality, and equal variance before t-test comparison. The goal of the two-sample t-test was to begin investigating whether or not the mean water isotope values from ice lenses are significantly similar to or different from the surrounding snow samples.

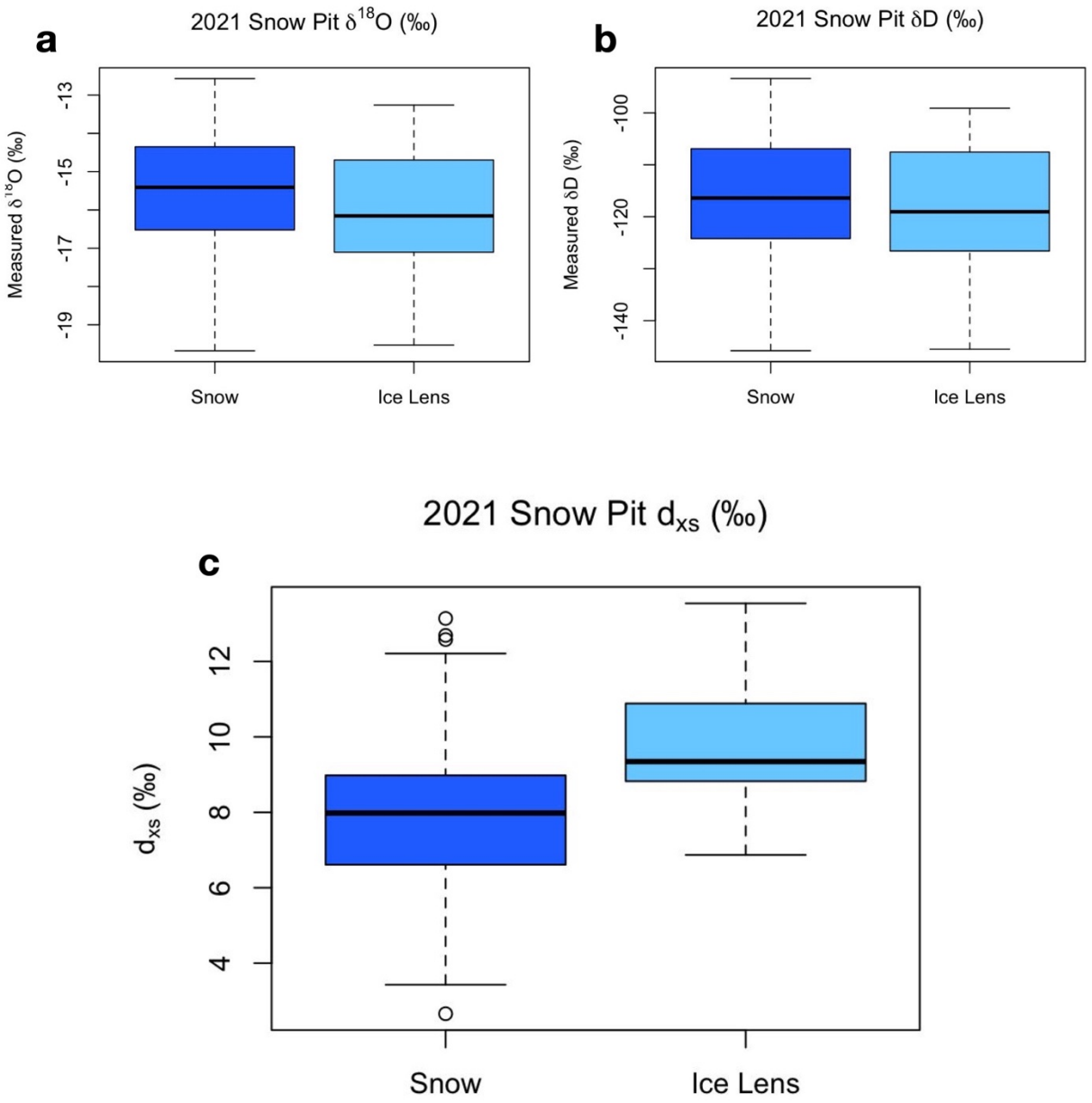

Figure 9: Mean $\delta^{18}O$, δD, and d_{xs} values for snow and ice lens samples from ten snow pits sampled throughout the 2021 JIRP field season.

Isotope Value	Snow Sample Mean (‰)	Ice Lens Sample Mean (‰)	t-value	DF	p-value
$\delta^{18}O$	-15.500	-15.96	1.241	139	0.2166
δD	-116.17	-117.95	0.629	139	0.5303
d_{xs}	7.8406	9.7270	-3.799	139	0.000217

Table 6: Results of three two-sample t-test to examine the sample mean equivalence of $\delta^{18}O$, δD, and d_{xs} in snow and ice lenses.

Discussion

This research explored two primary hypotheses – pre-depositional changes throughout water vapor transport or post-depositional changes within the firn aquifer – to explain the stable isotope anomalies in the upper 24.5m of the ML Ice Core. Water isotope anomalies within the ML Ice Core record were observed at and above the firn-ice transition (24.5m), where a firn aquifer was observed. We consider whether or not these anomalies could be linked to the presence of meltwater within the glacial ice or driven by atmospheric factors before precipitation. We first reconstructed three temperature parameters from the water isotope record using the SWIM model, which suggested an evaporation source temperature decrease of ~5˚C (see Fig. 8). Using a modeled depth-age relationship that estimated the firn-ice transition at ~10ya (see Fig. 4), we next examined sea surface temperatures from the past 20-30 years using NCEP reanalysis data to explore whether or not SST shifts could be causing the evaporative source reconstruction suggested by SWIM (see Fig. 9). To understand precipitation patterns on the JIF in relation to SST, we then clustered two years (2008 and 2010) of HySPLIT modeled air parcel back-trajectories and overlayed the projected water vapor pathways on the reconstructed SST maps with the hope of constraining the snow that fell at the depth of the firn-ice transition (see Fig. 9). Our results indicate that the water isotope anomalies present within the upper 24.5m of the ML Ice Core are not likely linked to the evaporation source temperature shifts, either from SST changes or storm pathway alterations. Thus, they are perhaps the result of post-depositional processes linked to meltwater, including percolation, refreezing, and/or fractionation.

Ice Core Water Isotope Analysis

The water isotope anomalies present at 20.75m and 24.25m are shown in Figures 2 and 5, and could be signals of extreme seasonal variability, hydrologic cycle alteration, sea surface temperature shifts, or post-depositional processes. Above these anomalous measurements, the water isotope record displays wider variability and slightly higher (less negative) mean $\delta^{18}O$ and δD values (see Table 2). Table 2 shows that the two anomalies did not impact the mean water isotope values drastically, though the standard deviations shifted as a response. Because water isotopes are considered temperature proxies, the anomalously low $\delta^{18}O$ and δD values at 20.75m ($\delta^{18}O = –20.032‰$, $\delta D = –145.83‰$) could be linked to a very cold precipitation event or season, while the anomalously high $\delta^{18}O$ and δD values at 24.25m ($\delta^{18}O = –10.931‰$, $\delta D = –105.3‰$) could be the result of a warmer storm event (Dansgaard, 1964; Jouzel & Merlivat, 1984; Rozanski et al, 1993). Liquid water table measurements from the borehole are displayed by the pink dashed line in Figure 2 and fall near the measured water isotope values at 20.75m, perhaps indicating that liquid water has affected the lower anomaly in question ($\delta^{18}O = –20.032‰$, $\delta D = –145.83‰$). Seasonal or storm-specific temperature variability is not further considered as a cause of the

anomalies because the SWIM condensation site and surface temperature reconstructions do not indicate extraordinary temperatures (see Fig. 8). Rather, we use the subsequent sections to interpret the role of evaporation source temperatures, sea surface temperatures, and post-depositional processes as the main drivers.

SWIM Temperature Reconstructions

SWIM reconstructs evaporation source temperature (T_{evap}), condensation site temperature (T_{cond}), and condensation surface temperature ($T_{surface}$) for given starting conditions and water isotope data inputs. Figure 8 displays the T_{evap}, T_{cond}, and $T_{surface}$ reconstructed temperatures for the ML Ice Core record and shows that the precipitation in the upper 24.5m perhaps originated from a temperature ~5˚C cooler than the precipitation that accumulated below the firn-ice transition. In order for an origin temperature to be ~5˚C cooler, the source body of water could have decreased, or the location of evaporation could have changed (Markle & Steig, 2022). This temperature shift seems unlikely when compared to the T_{evap} throughout the ice core depth, because the remaining 269.5m of the ice below the firn-ice transition has a mean T_{evap} of approximately 15.5˚C (see Table 3). We explored the validity of the SWIM output through a combination of SST analysis and air parcel trajectory modeling before ruling out the possibility of evaporative temperature shift, though it is most likely that the SWIM model outputs were altered by the water isotope anomalies. Within the scope of this study, we aimed to verify whether or not the SWIM evaporation temperature reconstructions are a likely cause of the water isotope data anomalies.

SST Reconstructions and Air Parcel Back-Trajectories

The combined analysis of the HYSPLIT back-trajectories and SST reconstructions show no large shift in air parcel transport pathways before and after the firn-ice transition, and no temperature shift in the mean winter sea surface temperatures on the order of 5˚C throughout the past 20 years. It is thus unlikely that the SWIM outputs suggesting a T_{evap} downward shift of ~5˚C is the cause of the water isotope anomalies observed. We used an approximate depth-age relationship for the firn-ice transition (2009) to model air parcel back-trajectories using the NOAA HYSPLIT model for the two years (2008 and 2010) on either side of the firn-aquifer age, then compared clustered water vapor transport pathways to the long term mean SST (1990-2020) and SST anomaly from 2000-2020. HYSPLIT outputs (Figure 9) indicate that the average moisture source to the Juneau Icefield did not shift from 2008 to 2010, with a majority of the water vapor originating in the Pacific Basin (>40˚N) and Bering Sea (>52˚N). SST reanalysis outputs are displayed in Figure 9. Panel a) displays the SST anomaly calculated by subtracting the mean winter SST from 2000-2010 from the mean winter SST from 2010-2020. It reveals that between 2010 and 2020, the Arctic Ocean warmed by ~1-2˚C relative to 2000-2010 mean SST, and the Pacific

Basin temperature fluctuated approximately ±0.5˚C relative to the same time period. Panel b) and c) show the 2008 and 2010 HySPLIT back trajectories projected on the long-term mean absolute SST. Neither of the SST reconstructions show the 5˚C temperature decrease that SWIM suggested for the snow and firn source evaporation temperature (see Fig. 9). We therefore conclude that the HYSPLIT back-trajectories and SST reconstructions do not validate the SWIM evaporation source temperature theory of a 5˚C cold shift.

2021 Sample Analysis

Preliminary examination of the water isotope composition of ice lenses and snow samples from snow pits across the Juneau Icefield during the 2021 season revealed that there is no significant difference between the mean $\delta^{18}O$ and δD of the snow and ice lenses ($t = 1.2411$, $t = 0.6292$, $p>0.05$), but that there is a significant difference between the d_{xs} values of the snow and ice lenses ($t = –3.7987$, $p<0.05$). On the Juneau Icefield, ice lenses are likely records of winter/spring melt and refreeze processes, because it is unlikely that summer temperatures are conducive to meltwater refreezes during percolation through the snow pack. Additionally, ice lenses are formed through the process of melt and refreeze, and are potential sources of fractionation as a result of phase changes. Meltwater percolation in glacial ice has the potential to wash-out and obscure the water isotope signal (Koerner, 1997; Neff et al., 2012; Schotterer et al., 2004), enrich the heavy isotopes preserved water isotope record, or lead to post-depositional fractionation through refreezing processes (Moran & Moran, 2009; Pu et al., 2020; Taylor et al., 2001). Statistical analysis of ice lenses within snow pits showed that mean d_{xs} values in snow and ice lenses are significantly different, and that the mean d_{xs} of ice lenses within the same snowpack is approximately 2‰ higher (see Fig. 11 and Table 6). The fact that ice lenses have higher d_{xs} values than the surrounding snow may indicate that isotopic exchange is occurring through the process of melt and refreeze, though this sample size is not large enough to draw such conclusions. Ice lens analysis is interesting in the context of the firn aquifer because ice lenses form through the process of melt and refreeze, and may shed light on the processes occurring within the liquid water of the ML Ice Core.

Limitations

This research is limited in a few aspects, which should be considered when interpreting the results. There is the potential for the water isotope data anomalies to be the result of measurement error or sampling error. With regards to the SWIM model, limitations arise because the model does not account for the possibility of post-depositional processes occurring englacially, and hence cannot differentiate between an atmospheric shift and one happening within the snow-ice interface (Markle & Steig, 2022). Furthermore, the SWIM model was written and designed for Antarctic applications and may inaccurately

represent Northern hemispheric conditions. These two complexities may be driving the difference in evaporation source temperature reconstruction, and should be explored in further studies. The NOAA HySPLIT back-trajectories are a result of many mathematical approximations that aim to estimate physical processes such as evaporation, diffusion, and hence numerical calculations are a large source of uncertainty in the outputs (Harris et al., 2005; Markle et al., 2012). Furthermore, HySPLIT uncertainty is complicated by the resolution of the NCEP reanalysis data at mid to high latitudes (Bromwich & Fogt, 2004; Markle et al., 2012). Similarly, the NOAA/NCEP sea surface temperature analysis is dependent on NCEP reanalysis data with the same resolution. Regarding the 2021 JIRP data, snow and ice lens sample analysis from the 2021 field season is limited by the fieldwork season timeline (June to August). During the summer months, the ablation season is well underway; thus, some of the season's accumulated snow has melted or sublimated and is not represented by the measured samples. Furthermore, one season of empirical data is not extensive enough to draw conclusions about long-term trends or processes. Rather, the goal with the 2021 sample analysis was to begin preliminary examination of phase change dynamics and their potential impact on measured water isotope signatures.

Conclusion

The ML Ice Core, drilled in 2019 on the Juneau Icefield, Alaska, presented anomalous stable water isotope values that coincide with the presence of liquid water in a ~5cm thick firn aquifer, 24.5m from the surface of the ice. Combined air parcel back-trajectory modeling and sea surface temperature analysis do not support the hypothesis that evaporative source temperature shifts caused the water isotope anomalies at and above the firn-ice transition, thus suggesting that post-depositional processes occurring englacially possible led to the observed data spikes. Analysis of ten 2021 JIRP snow pits showed that there is no significant difference between the mean $\delta^{18}O$ and δD of the snow and ice lenses, but that the mean d_{xs} of ice lenses within the same snowpack is approximately 2‰ higher than the snow. There are five potential directions for the future of this study. First, existing snow pit, shallow core, and surface transect data across the Juneau Icefield spans the years of 2012 to 2022, and should be assessed for signals of meltwater driven post-depositional process. This analysis could include mutli-year ice lens water isotope analysis, meltwater isotope comparison to the firn aquifer, kinetic fractionation modeling, and broader water isotope variability analysis. Second, HySPLIT back-trajectory analysis could be expanded to examine daily trajectories for all years from 2000-2020 and long-term trends in water vapor transport pathways. Third, water isotope composition from melt layers in nearby ice cores could be compared to the JIRP snow sample dataset, and ML Ice Core firn aquifer anomalies, where records are available. Fourth, controlled lab experiments could be performed to simulate melt-refreeze fractionation dynamics. Hughes et al. (2021) used a controlled lab environment to experiment with sublimation-driven

post-depositional water isotope processes, and a similar process could be applied to meltwater dynamics. Last, to gain a deeper understanding of the water isotope geochemistry of the Matthes-Llewelyn ice divide and broader Juneau Icefield, another deep ice core should be drilled at the ice divide and processed to study chemical signals beyond water isotopes. With an additional deep ice core at the ML Divide, a higher resolution water isotope record could be assessed alongside other signals such as dust particulates, volcanic ash deposits, and greenhouse gas bubbles, to produce a better constrained depth-age relationship and climate record for the Juneau Icefield.

Acknowledgements

This research project is overseen by Bradley Markle, PhD, assistant professor at the Institute of Arctic and Alpine Research's (INSTAAR) Stable Isotope Lab and in the Department of Geological Sciences at CU Boulder, as well as the assistant academic director of the Juneau Icefield Research Project. Dr. Markle has also managed the JIRP Water Isotope project since 2012, when the spatial analysis began. Isotope data since 2012 has been analyzed in the field and at the University of Alaska Anchorage by Eric Klein. TJ Fudge at the University of Washington provided the code for the DJ model, Seth Campbell provided GPR transect information at the ML Ice Core drill site, and Chris McNeil provided snow accumulation information specific to the Juneau Icefield. 2021 data collection was made possible by the student research team; Liam Kirkpatrick (Dartmouth), Michela Savignano (Brown), Abby Holt (Principia), and Nicholas Bakken-French (Whittier). Samples were run at the Stable Isotope Laboratory at INSTAAR with the assistance of lab technician Valerie Morris. The Undergraduate Research Opportunities Program (UROP) at CU Boulder has funded this project for two academic years. Additional fieldwork funding for JIRP came from the Foundation for Glacier and Environmental Research. Lastly, this project would not be here without Moria Torrington, at the CU Boulder Writing Center, who has spent countless hours over the past two years helping me consolidate these ideas onto paper.

References

Anderson, R. S., & Anderson, S. P. (2010). *Geomorphology*. Cambridge University Press.

Arendt, A. A., Echelmeyer, K. A., Harrison, W. D., Lingle, C. S., & Valentine, V. B. (2002). Rapid Wastage of Alaska Glaciers and Their Contribution to Rising Sea Level. *Science*, *297*(5580), 382–386. https://doi.org/10.1126/science.1072497

Baker, E. H., McGee, S., Campbell, S. W., Pierce, J. L., & Mcneil, C. J. (2019). *Weather Station Data on the Juneau Icefield* [Csv,zip]. U.S. Geological Survey. https://doi.org/10.5066/P9DUI71J

Bromwich, D. H., & Fogt, R. L. (2004). Strong Trends in the Skill of the ERA-40 and NCEP–NCAR Reanalyses in the High and Midlatitudes of the Southern Hemisphere, 1958–2001. *Journal of Climate*, *17*(23), 4603–4619. https://doi.org/10.1175/3241.1

Brönnimann, S. (2020). *Climate of the Free Troposphere and Mountain Peaks*. Oxford University Press. https://doi.org/10.1093/acrefore/9780190228620.013.755

Casado, M., Landais, A., Picard, G., Arnaud, L., Dreossi, G., Stenni, B., & Prié, F. (2021). Water Isotopic Signature of Surface Snow Metamorphism in Antarctica. *Geophysical Research Letters*, *48*(17), e2021GL093382. https://doi.org/10.1029/2021GL093382

Clifford, H. M., Spaulding, N. E., Kurbatov, A. V., More, A., Korotkikh, E. V., Sneed, S. B., Handley, M., Maasch, K. A., Loveluck, C. P., Chaplin, J., McCormick, M., & Mayewski, P. A. (2019). A 2000 Year Saharan Dust Event Proxy Record from an Ice Core in the European Alps. *Journal of Geophysical Research: Atmospheres*, *124*(23), 12882–12900. https://doi.org/10.1029/2019JD030725

Coplen, T.B., Hopple, J.A., Böhlke, J.K., Peiser, H.S., Rieder, S.E., Krouse, H.R., Rosman, K.J.R., Ding, T., Vocke, R.D.J., Révész, K.M., Lamberty, A., Taylor, P. and DeBièvre, P. (2002) Compilation of Minimum and Maximum Isotope Ratios of Selected Elements in Naturally Occurring Terrestrial Materials and Reagents. United States Geological Survey, Reston, p. 98. https://doi.org/10.3133/wri014222

Dansgaard, W. (1964). Stable isotopes in precipitation. *Tellus*, *16*(4), 436–468. https://doi.org/10.3402/tellusa.v16i4.8993

Dansgaard, W., & Johnsen, S. J. (1969). A Flow Model and a Time Scale for the Ice Core from Camp Century, Greenland. *Journal of Glaciology*, *8*(53), 215–223. https://doi.org/10.3189/S0022143000031208

Draxler, R. R., & Hess, G. D. (1998). *An Overview of the HYSPLIT_4 Modelling System for Trajectories, Dispersion, and Deposition*.

Dorling, S. R., Davies, T. D., & Pierce, C. E. (1992). Cluster analysis: A technique for estimating the synoptic meteorological controls on air and precipitation chemistry—Method and applications. *Atmospheric Environment. Part A. General Topics*, *26*(14), 2575–2581. https://doi.org/10.1016/0960-1686(92)90110-7

Fang, L., Jenk, T. M., Singer, T., Hou, S., & Schwikowski, M. (2021). Radiocarbon dating of alpine ice cores with the dissolved organic carbon (DOC) fraction. *The Cryosphere*, *15*(3), 1537–1550. https://doi.org/10.5194/tc-15-1537-2021

Gat, J. R. (1996). *OXYGEN AND HYDROGEN ISOTOPES IN THE HYDROLOGIC CYCLE*.

Harris, J. M., Draxler, R. R., & Oltmans, S. J. (2005). Trajectory model sensitivity to differences in input data and vertical transport method. *Journal of Geophysical Research: Atmospheres*, *110*(D14). https://doi.org/10.1029/2004JD005750

Hooijer, A., & Vernimmen, R. (2021). Global LiDAR land elevation data reveal greatest sea-level rise vulnerability in the tropics. *Nature Communications*, *12*(1), 3592. https://doi.org/10.1038/s41467-021-23810-9

Juneau Icefield Research Program. (n.d.). Retrieved October 18, 2021, from https://juneauicefield.org/

Jouzel, J., & Merlivat, L. (1984). Deuterium and oxygen 18 in precipitation: Modeling of the isotopic effects during snow formation. *Journal of Geophysical Research: Atmospheres*, *89*(D7), 11749–11757. https://doi.org/10.1029/JD089iD07p11749

Jouzel, J., Alley, R. B., Cuffey, K. M., Dansgaard, W., Grootes, P., Hoffmann, G., Johnsen, S. J., Koster, R. D., Peel, D., Shuman, C. A., Stievenard, M., Stuiver, M., & White, J. (1997). Validity of the temperature reconstruction from water isotopes in ice cores. *Journal of Geophysical Research: Oceans*, *102*(C12), 26471–26487. https://doi.org/10.1029/97JC01283

Kalnay, E. and Coauthors, 1996: The NCEP/NCAR Reanalysis 40-year Project. Bull. Amer. Meteor. Soc., 77, 437-471.

Klein, E. S., Nolan, M., McConnell, J., Sigl, M., Cherry, J., Young, J., & Welker, J. M. (2016). McCall Glacier record of Arctic climate change: Interpreting a northern Alaska ice core with regional water isotopes. *Quaternary Science Reviews*, *131*, 274–284. https://doi.org/10.1016/j.quascirev.2015.07.030

Lemieux-Dudon, B., Blayo, E., Petit, J.-R., Waelbroeck, C., Svensson, A., Ritz, C., Barnola, J.-M., Narcisi, B. M., & Parrenin, F. (2010). Consistent dating for Antarctic and Greenland ice cores. *Quaternary Science Reviews*, *29*(1), 8–20. https://doi.org/10.1016/j.quascirev.2009.11.010

Lliboutry, L. (1979). A Critical Review Of Analytical Approximate Solutions For Steady State Velocities And Temperatures In Cold Ice-Sheets. *A Critical Review Of Analytical Approximate Solutions For Steady State Velocities And Temperatures In Cold Ice-Sheets*, 15(2), 135–148.

L2130-i Isotope and Gas Concentration Analyzer | Picarro. (n.d.). Retrieved December 7, 2021, from https://www.picarro.com/products/l2130i_isotope_and_gas_concentration_analyzer

Markle, B. R., Bertler, N. A. N., Sinclair, K. E., & Sneed, S. B. (2012). Synoptic variability in the Ross Sea region, Antarctica, as seen from back-trajectory modeling and ice core analysis: SYNOPTIC VARIABILITY IN ICE CORE RECORDS. *Journal of Geophysical Research: Atmospheres*, *117*(D2), n/a-n/a. https://doi.org/10.1029/2011JD016437

Markle, B. R., Steig, E. J., Buizert, C., Schoenemann, S. W., Bitz, C. M., Fudge, T. J., Pedro, J. B., Ding, Q., Jones, T. R., White, J. W. C., & Sowers, T. (2017). Global atmospheric teleconnections during Dansgaard–Oeschger events. *Nature Geoscience*, *10*(1), Article 1. https://doi.org/10.1038/ngeo2848

Markle, B. R., & Steig, E. J. (2022). Improving temperature reconstructions from ice-core water-isotope records. *Climate of the Past*, *18*(6), 1321–1368. https://doi.org/10.5194/cp-18-1321-2022

Mark II Ice Coring System | Kovacs Enterprise. (n.d.). Retrieved December 8, 2021, from https://kovacsicedrillingequipment.com/coring-systems/mark-ii/

Martini, I. P., Brookfield, M. E., & Sadura, S. (2001). *Principles of Glacial Geomorphology and Geology*. Prentice Hall.

Moran, T., & Marshall, S. (2009). The effects of meltwater percolation on the seasonal isotopic signals in an Arctic snowpack. *Journal of Glaciology*, *55*(194), 1012–1024. https://doi.org/10.3189/002214309790794896

Nardin, R., Severi, M., Amore, A., Becagli, S., Burgay, F., Caiazzo, L., Ciardini, V., Dreossi, G., Frezzotti, M., Hong, S.-B., Khan, I., Narcisi, B. M., Proposito, M., Scarchilli, C., Selmo, E., Spolaor, A., Stenni, B., & Traversi, R. (2021). *Dating of an East Antarctic ice core (GV7) by high resolution chemical stratigraphies*. https://doi.org/10.5194/cp-2021-44

Neff, P. D., Steig, E. J., Clark, D. H., McConnell, J. R., Pettit, E. C., & Menounos, B. (2012). Ice-core net snow accumulation and seasonal snow chemistry at a temperate-glacier site: Mount Waddington, southwest British Columbia, Canada. *Journal of Glaciology*, *58*(212), 1165–1175. https://doi.org/10.3189/2012JoG12J078

Nolan, M., Motkya, R. J., Echelmeyer, K., & Trabant, D. C. (1995). Ice-thickness measurements of Taku Glacier, Alaska, U.S.A., and their relevance to its recent behavior. *Journal of Glaciology*, *41*(139), 541–553. https://doi.org/10.3189/S0022143000034870

Pelto, M. S., Miller, M. M., Adema, G. W., Beedle, M. J., McGee, S. R., Sprenke, K. F., & Lang, M. (2008). The equilibrium flow and mass balance of the Taku Glacier, Alaska 1950–2006. *The Cryosphere*, 11.

Rozanski, K., Araguás-Araguás, L., & Gonfiantini, R. (1993). Isotopic Patterns in Modern Global Precipitation. In P. K. Swart, K. C. Lohmann, J. Mckenzie, & S. Savin (Eds.), *Geophysical Monograph Series* (pp. 1–36). American Geophysical Union. https://doi.org/10.1029/GM078p0001

Shao, L., Tian, L., Wu, G., Naftz, D., Cai, Z., Wang, C., Li, Y., & Palcsu, L. (2020). Dating of an alpine ice core from the interior of the Tibetan Plateau. *Quaternary International*, *544*, 88–95. https://doi.org/10.1016/j.quaint.2020.02.030

Sharp, Z. (2017). *Principles of Stable Isotope Geochemistry, 2nd Edition*. https://digitalrepository.unm.edu/unm_oer/1

Stein, A. F., Draxler, R. R., Rolph, G. D., Stunder, B. J. B., Cohen, M. D., & Ngan, F. (2015). NOAA's HYSPLIT Atmospheric Transport and Dispersion Modeling System. *Bulletin of the American Meteorological Society*, *96*(12), 2059–2077. https://doi.org/10.1175/BAMS-D-14-00110.1

Tianming Ma, Li Li, Guitao Shi, & Yuansheng Li. (2020). Acquisition of Post-Depositional Effects on Stable Isotopes (δ18O and δD) of Snow and Firn at Dome A, East Antarctica. *Water*, *12*(6). https://doi.org/10.3390/w12061707

Tiwari, M., Singh, A. K., & Sinha, D. K. (2015). Chapter 3 - Stable Isotopes: Tools for Understanding Past Climatic Conditions and Their Applications in Chemostratigraphy. In Mu. Ramkumar (Ed.), *Chemostratigraphy* (pp. 65–92). Elsevier. https://doi.org/10.1016/B978-0-12-419968-2.00003-0

Uemura, R., Masson-Delmotte, V., Jouzel, J., Landais, A., Motoyama, H., & Stenni, B. (2012). Ranges of moisture-source temperature estimated from Antarctic ice cores stable isotope records over glacial–interglacial cycles. *Climate of the Past*, *8*(3), 1109–1125. https://doi.org/10.5194/cp-8-1109-2012

What is Paleoclimatology? | National Centers for Environmental Information (NCEI) formerly known as National Climatic Data Center (NCDC). (n.d.). Retrieved December 7, 2021, from https://www.ncdc.noaa.gov/news/what-paleoclimatology

White, W. M. (2015). *Isotope Geochemistry*. John Wiley & Sons, Incorporated.

Winski, D., Osterberg, E., Kreutz, K., Wake, C., Ferris, D., Campbell, S., Baum, M., Bailey, A., `Birkel, S., Introne, D., & Handley, M. (2018). A 400-Year Ice Core Melt Layer Record of Summertime Warming in the Alaska Range. *Journal of Geophysical Research: Atmospheres*, *123*(7), 3594–3611. https://doi.org/10.1002/2017JD027539

Zemp, M., Huss, M., Thibert, E., Eckert, N., McNabb, R., Huber, J., Barandun, M., Machguth, H., Nussbaumer, S. U., Gärtner-Roer, I., Thomson, L., Paul, F., Maussion, F., Kutuzov, S., & Cogley, J. G. (2019). Global glacier mass changes and their contributions to sea-level rise from 1961 to 2016. *Nature*, *568*(7752), 382-386,386A-386L. http://dx.doi.org/10.1038/s41586-019-1071-0